

This is the author's final version of the contribution published as:

Luca Barale, Carlo Bertok, Namam Salih Talabani, Anna d'Atri, Luca Martire, Fabrizio Piana, Alain Pr  at. Very hot, very shallow hydrothermal dolomitization: An example from the Maritime Alps (north-west Italy–south-east France). *SEDIMENTOLOGY*. None pp: 1-29.
DOI: doi: 10.1111/sed.12294

When citing, please refer to the published version.

Link to this full text:

<http://hdl.handle.net/>

1VERY HOT, VERY SHALLOW HYDROTHERMAL DOLOMITIZATION: AN EXAMPLE FROM 2THE MARITIME ALPS (NW ITALY – SE FRANCE)

3

4Luca Barale^{1*}, Carlo Bertok¹, Namam Salih Talabani^{2,3}, Anna d'Atri¹, Luca Martire¹, Fabrizio
5Piana⁴, Alain Pr  at²

6

7

81: Dipartimento di Scienze della Terra, Universit   di Torino, Via Valperga Caluso 35, 10125
9Torino.

102: Department of Earth and Environmental Sciences, Universit   Libre de Bruxelles, 50, avenue
11F. D. Roosevelt, CP 160/02. B-1050 Brussels. Belgium.

123: Petroleum Geosciences Department, Soran University, Delizian, Soran/Erbil, Iraq-Kurdistan.

134: CNR IGG – Torino, Via Valperga Caluso 35, 10125 Torino.

14* Corresponding author. E-mail: luca.barale@hotmail.it

15

16*Running head: Very hot, very shallow hydrothermal dolomitization*

17

18ABSTRACT

19In the Maritime Alps (NW Italy–SE France), the Middle Triassic–lowermost Cretaceous platform
20carbonates of the Proven  al Domain locally show an intense dolomitization. Dolomitized bodies,
21irregularly shaped and variable in size from some metres to hundreds of metres, are associated
22with tabular bodies of dolomite-cemented breccias, cutting the bedding at a high angle, and
23networks of dolomite veins. Field and petrographic observations indicate that dolomitization was
24a polyphase process, in which episodes of hydrofracturing and host-rock dissolution, related to
25episodic expulsion of overpressured fluids through faults and fracture systems, were associated
26with phases of host-rock dolomitization and void cementation. Fluid inclusion analysis indicates
27that dolomitizing fluids were relatively hot (170–260   C). The case study represents an
28outstanding example of a fossil hydrothermal system, which significantly contributes to the
29knowledge of such dolomitization systems in continental margin settings. The unusually
30favourable stratigraphic framework allows precise constraint of the timing of dolomitization
31(earliest Cretaceous), and, consequently, direct evaluation of the burial setting of dolomitization,
32which, for the upper part of the dolomitized succession, was very shallow or even close to the
33surface. The described large-scale hydrothermal system was probably related to deep-rooted

34 faults, and provides indirect evidence of a significant earliest Cretaceous fault activity in this part
35 of the Alpine Tethys European palaeomargin.

36

37 *Keywords: hydrothermal dolomitization, fault-related fluid circulation, Early Cretaceous,*

38 *Provençal Domain, Maritime Alps*

39

40 INTRODUCTION

41 In the broad field of dolomite literature, hydrothermal dolomitization processes (sensu Machel
42 and Lonnee, 2002; Machel, 2004; Davies and Smith, 2006) represent the most studied and
43 discussed in recent years. In fact, beyond the scientific significance, hydrothermal dolostones
44 also have a high economic value, as they have long been known to host important base metal
45 mineralizations (e.g. Mississippi Valley-Type lead–zinc ores; Hewett, 1928). More recently they
46 have been recognized as potentially good hydrocarbon reservoirs (Davies and Smith, 2006,
47 and references therein). Moreover, the upflow of high-temperature fluids through a column of
48 sediments can force the maturation of the organic matter and influence the migration of
49 hydrocarbons (e.g. Lavoie *et al.*, 2005; Sharp *et al.*, 2010; Guo *et al.*, 2011).

50 In recent years, many examples of hydrothermal dolomitization have been documented
51 worldwide (e.g. Boni *et al.*, 2000; Laponi *et al.*, 2007, 2014; López-Horgue *et al.*, 2010; Nader
52 *et al.*, 2012; Swennen *et al.*, 2012; Haeri-Ardakani *et al.*, 2013a, b; Hendry *et al.*, 2015). In the
53 Alpine chain, several examples of hydrothermal dolomitization come from the Southern Alps
54 (Spencer-Cervato and Mullis, 1992; Carmichael and Ferry, 2008; Carmichael *et al.*, 2008; Ferry
55 *et al.*, 2011; Ronchi *et al.*, 2011, 2012). In many of these study cases, the most challenging
56 point is the timing and the burial depth of dolomitization, which can be only inferred on the basis
57 of indirect evidence regarding the regional context and the burial history.

58 In the Maritime Alps (NW Italy–SE France), the Middle Triassic and the Middle Jurassic–
59 Berriasian carbonates of the Provençal Domain are locally affected by intense dolomitization in
60 an area of some tens of square kilometres, between the Vermentina, Gesso, and Sabbione
61 valleys to the north and the Roya and Bieugne valleys to the south (Fig. 1, 2). The presence of
62 these dolostones has already been reported, although very briefly, by Bigot *et al.* (1967),
63 Campanino Sturani (1967), Carraro *et al.* (1970), and Malaroda (1970, 1999). A preliminary
64 description of this phenomenon has been given by Barale *et al.* (2013a), who documented its
65 hydrothermal character, whereas Barale *et al.* (2016) mapped the distribution of dolomitization
66 in the Italian part of the study area. The aim of this paper is to provide the full dataset of field,

67 petrographic, and geochemical characteristics of this remarkable study case of hydrothermal
68 dolomites. The broad significance of this study case derives from the following points:

69

70- local stratigraphy strictly constrains the timing and the burial depth of the dolomitization:
71 the latter is considerably shallower than those reported in previous literature cases;

72

73- inferred temperatures of dolomitizing fluids are very high, considering the shallow
74 subsurface dolomitization environment; and

75

76- it is the first report of hydrothermal dolomite in the Western Alps, where it contributes to
77 a better knowledge of an Early Cretaceous syndepositional tectonics.

78

79 GEOLOGICAL SETTING

80 The Mesozoic succession of the study area was deposited on the European palaeomargin of
81 the Alpine Tethys, in the northern part of the Provençal platform, close to the transition to the
82 Dauphinois basin (Carraro *et al.*, 1970; Lanteaume 1990; Barale *et al.*, 2016; d'Atri *et al.*, 2016).
83 The Provençal succession starts with Permian continental sediments resting on the crystalline
84 basement of the Argentera Massif, characterized by marked changes in thickness and reaching
85 a maximum thickness of 3000–4000 metres (Faure-Muret, 1955). They are followed by some
86 tens of metres of Lower Triassic coastal siliciclastic deposits, Middle Triassic peritidal
87 carbonates, a few hundred metres thick, and Upper Triassic evaporites. Discrete stratigraphic
88 intervals of Middle Triassic carbonates consist of finely crystalline dolostones that are
89 widespread at the regional scale (e.g., Lanteaume, 1968; Carraro *et al.*, 1970; Costamagna,
90 2013). A regional discontinuity surface corresponding to a Late Triassic–Early Jurassic hiatus is
91 followed by 200–300 m of platform limestones attributed to the Middle Jurassic–Berriasian
92 (Garbella Limestone; Barale, 2014; Barale *et al.*, 2016). Lower Cretaceous deposits are
93 represented by a condensed succession of bioclastic limestones and marly limestones, locally
94 rich in authigenic minerals (phosphates, glauconite), reaching a maximum thickness of some
95 tens of metres (Lanteaume, 1968; Malaroda, 1999; Barale *et al.*, 2013b). They are followed by
96 hemipelagic deposits of Late Cretaceous age. In the northern part of the study area (roughly
97 corresponding to the Italian part), Cretaceous deposits are in general thinner and locally absent
98 (Carraro *et al.*, 1970; Barale *et al.*, 2016). To the northwest of the study area, the Provençal
99 successions pass to thicker Dauphinois successions, characterized by several hundred metres
100 of pelagic to hemipelagic Jurassic–Cretaceous deposits (Carraro *et al.*, 1970; Barale *et al.*,

1012016). The transition between the Provençal platform and Dauphinois basin corresponds to a
102preserved primary feature (Caire Porcera palaeomargin), which originated as a fault-related
103palaeo-escarpment during the Early–Middle Jurassic and was subsequently covered by
104Cretaceous slope deposits (Barale, 2014; Barale *et al.*, 2016; d'Atri *et al.*, 2016). The top of the
105Mesozoic succession is truncated by a regional unconformity, corresponding to a hiatus
106spanning the latest Cretaceous–middle Eocene, overlain by the Alpine Foreland Basin
107succession. This consists of middle Eocene Nummulitic Limestone (mixed carbonate–
108siliciclastic ramp deposits), followed by the hemipelagic upper Eocene *Globigerina* Marl and by
109the upper Eocene–lower Oligocene turbidite succession of the Grès d'Annot (Sinclair, 1997).
110Since the Eocene, the palaeo-European continental margin has been progressively involved in
111the ongoing formation of the Alpine belt (e.g., Dumont *et al.*, 2012). All the study successions
112underwent at least three deformation events that were well recorded at a regional scale, firstly
113with outward (southwestward) brittle–ductile thrusting and superposed foldings, then
114northeastward back-vergent folding, and lastly southward brittle thrusting and flexural folding
115(d'Atri *et al.*, 2016). The regional structural setting resulted from a transpressional regime with
116important strain partitioning of contractional versus strike-slip-related structural associations
117(Piana *et al.*, 2009; d'Atri *et al.*, 2016), as evidenced by the occurrence of a post-Oligocene
118NW–SE Alpine transcurrent shear zone (Limone Viozene Zone) extending for several kilometres
119from Tanaro valley to the study area. This shear zone is probably superimposed on a long-lived
120shearing corridor active since the Jurassic–Cretaceous and reactivated during the Cenozoic
121(Bertok *et al.*, 2012; d'Atri *et al.*, 2016). Stratigraphic and geometric evidence of Cretaceous
122paleofaults have been locally described in nearby sectors (e.g. Bertok *et al.*, 2012), but
123commonly, in the study area, the large amount of finite deformation related to Alpine tectonics
124hinders direct recognition of ancient structures. Hydrothermal dolomitization affects the whole
125Provençal succession from the Middle Triassic carbonates to the Middle Jurassic–Berriasian
126shallow-water Garbella Limestone (Fig. 3). The Middle Triassic carbonates are represented by a
127150–200-m-thick succession of limestones, dolomitic limestones, and fine-grained dolostones,
128with decimetre-thick bedding (Bersezio and d'Atri, 1986; Malaroda, 1999). Common
129sedimentary structures are microbial/algal lamination, collapse breccias, flat pebble breccias,
130tepees, and millimetre-sized calcite pseudomorphs on gypsum crystals, all reflective of a
131peritidal depositional environment. An interval of dark-coloured, organic-rich limestones and
132dolostones, a few tens of metres thick, is locally present above the Middle Triassic carbonates
133(Mont Chajol, see Fig. 2) and is attributed to the Upper Triassic (Malaroda, 1999).

The Garbella Limestone is a 200–300-m-thick platform succession organized in poorly-defined decimetre- to metre-thick beds and mainly consisting of bioclastic packstones to rudstones and boundstones, rich in echinoderm fragments, corals, nerineid gastropods (e.g. *Ptygmatis pseudobruntrutana*), rudists (Diceratidae), and stromatoporoids. In the upper part, bioclastic mudstones–wackestones with *Clypeina jurassica* are common. The uppermost 5–10 metres are locally represented by peritidal limestones associated with lagoonal charophyte-rich wackestones, of supposed Berriasian age (Barale, 2014; Barale *et al.*, 2016). In the Mont Chajol sector, the Middle–Upper Jurassic succession is formed by micritic limestones with *Saccocoma* and ammonites, attributed to a more pelagic environment with respect to the carbonates of the adjoining sectors. They locally contain beds of oolitic grainstones, interpreted as resedimented deposits.

145

146 METHODS

Petrographic studies on 70 uncovered thin sections (30 µm thick) were carried out by optical microscopy and cathodoluminescence (CL) with the aim of distinguishing different dolomite generations. CL observations were carried out on polished thin sections using CITL 8200 mk3 equipment (operating conditions of about 17 kV and 400 µA). In situ quantitative microprobe analyses were performed on carbon-coated thin sections with an energy dispersive x-ray spectroscopy (EDS) Energy 200 system and a Pentafet detector (Oxford Instruments) associated with a Cambridge Stereoscan S-360 scanning electron microscope (SEM). The operating conditions were 15 kV of accelerating voltage, around 1 nA of probe current, and 50 seconds of counting time. SEM–EDS quantitative data (spot size: 2 µm) were acquired and processed using the Microanalysis Suite Issue 12, INCA Suite version 4.01; Structure Probe, Inc. (SPI) natural mineral standards were used to calibrate the raw data; the RoPhiZeta correction (Pouchou and Pichoir, 1988) was applied. Analytical statistical errors Σ on atomic weight percent are 0.08 for Mg and Fe and 0.13 for Ca. Carbon and oxygen isotopic compositions of the carbonates were measured partly at the Stable Isotope Laboratory of the ETH Geological Institute, Zurich, Switzerland (using a Thermo Fisher Scientific GasBench II coupled to a Delta V mass spectrometer as described in Bretenbach and Bernasconi (2011)), and partly at the MARUM Stable Isotope Laboratory, Bremen, Germany (using a Finnigan MAT 252 mass spectrometer and following the standard method of McCrea (1950)). In both cases, the oxygen isotope composition of dolomite was calculated using the fractionation factor of Rosenbaum and Sheppard (1986). The isotopic ratios for carbon and oxygen are expressed as $\delta^{13}\text{C}$ and $\delta^{18}\text{O}$ per mil values relative to the VPDB (Vienna Pee Dee Belemnite) standard

168(precision $\pm 0.05\%$). Fluid inclusion petrography has been studied on bi-polished thin sections
 169(80 μm thick). Microthermometry of primary fluid inclusion assemblages on dolomite and calcite
 170was performed using a Linkam THMSG600 heating–freezing stage coupled with an Olympus
 171polarizing microscope (100 \times objective), using the standard method described by Goldstein and
 172Reynolds (1994). Crystal size classes used in dolomite description are those proposed by Folk
 173(1962).

174

175 **DOLOSTONE MAIN FEATURES**

176 **Geometry, distribution and structures of the dolomitized bodies**

177 Dolomitization affects the whole thickness of the Middle Triassic carbonates and of the overlying
 178 Garbella Limestone for a total thickness of about 400–500 m (Fig. 3). Sediments overlying the
 179 Garbella Limestone are not dolomitized, but they locally contain clasts of dolomitized rocks, as
 180 described below. In the study area, the Triassic–Jurassic succession shows different modes
 181 and degrees of dolomitization (Fig. 2). Dolomite occurs both as a replacement phase and as a
 182 void-filling cement. The term “dolomitization degree” is used here as a qualitative evaluation,
 183 considering the volumetric abundance of dolomite with respect to the host rock and the degree
 184 of overprint on the primary fabric. The highest degree is observed in a belt with a rough NW–SE
 185 orientation, about 2 km wide and 8–10 km long, extending from Punta Bussaia to the eastern
 186 side of the Sabbione Valley, and in the Mont Chajol–Mont Agnelet–Mont Paracouerte sector. In
 187 these areas dolomitization widely affects a great part of the Provençal carbonate succession
 188 (Fig. 4), and fabric-destructive facies are common, as well as breccias, dissolution cavities, and
 189 tightly spaced vein networks. Outside these areas, the dolomitization degree decreases: fabric-
 190 retentive facies prevail, whereas the fabric-destructive ones are limited to isolated masses of
 191 decimetre to metre size. Breccias and dissolution cavities are rare, and vein networks are more
 192 spaced. Similar dolomitization phenomena, though less intense, locally affect the Middle–Upper
 193 Jurassic and Berriasian limestones in other sectors of the Provençal Domain (southern side of
 194 Argentera Massif and Nice Arc: Dardeau and Bulard, 1978; Malaroda, 1999; Barale, 2014) (Fig.
 195 1955). In the Jurassic part of the succession, dolomitization gave rise mainly to light-coloured,
 196 intensely dolomitized bodies that are commonly irregularly shaped, vary in size from some
 197 decimetres to some hundred metres (Figs. 4, 6A), and show randomly oriented boundaries with
 198 the encasing limestones. Conversely, in the Triassic part of the succession, well exposed in the
 199 Mont Chajol–Mont Agnelet–Mont Paracouerte area, dark dolomite-cemented breccias prevail
 200 (Fig. 7) and light, pervasively dolomitized bodies are commonly limited to smaller masses,
 201 decimetre-thick and a few metres wide at most. They generally crosscut the host-rock bedding

202(Figs. 8A and C) but some stratabound occurrences have also been observed (Figs. 6B and
 2038B). The transition between completely dolomitized and undolomitized or poorly dolomitized rock
 204volumes is commonly very sharp and takes place in a few centimetres (Figs. 6B, 8A and C). In
 205the Garbella Limestone, bedding-parallel burial stylolites systematically cut through dolomite
 206crystals and veins (Fig. 9A).

207

208Dolomitization textures

209Partially dolomitized limestones constitute the greatest volume of the dolomitized rocks in the
 210study area. Four main types of partial-dolomitization fabrics can be distinguished:

211

- 212– Matrix-selective. Dolomitization of the matrix can be either partial or complete, but it
 213 affects the grains very marginally.
- 214 – Grain-selective. Dolomitization affects only the grains, or a particular kind of grain. This
 215 kind of selective dolomitization is commonly observed in the coarse-grained facies of the
 216 Garbella Limestone, where it typically affects large bioclasts in rudstones and
 217 boundstones (Fig. 9B) or ooids in oolitic grainstones.
- 218 – Non-selective. The host rock is partially replaced by medium to coarsely crystalline
 219 dolomite growing indifferently on the grains and on the matrix/cement of the rock
 220 (Fig. 10A).
- 221 – Veined limestones. Dolomitization develops along a vein network, with euhedral
 222 dolomite crystals spreading from the veins and substituting the surrounding rock (Fig.
 223 10B). Locally, a higher vein density is present within subvertical, centimetre- to
 224 decimetre-wide, tabular rock volumes (Fig. 10C). Veins are 200 μm to 2 mm thick on
 225 average and show a thin inner part (100–200 μm), composed of finely to medium
 226 crystalline turbid dolomite and a thicker outer part (100–1000 μm) composed of outward
 227 growing, coarse to very coarsely crystalline dolomite crystals (Fig. 10D and E). The latter
 228 grow as a replacement of the rock constituting the vein walls. Dolomite veins do not
 229 show any preferential orientation. These veins can be clearly distinguished from those
 230 related to Alpine structural associations, which commonly bear a large number of
 231 tectonic calcite veins both in fold-related settings and fracture networks. Furthermore,
 232 dolomite veins are systematically cut by a recurrent N–NE-striking system of tectonic
 233 calcite veins, widespread in the study area. A few isolated crystals can also occur in the
 234 host rock, far from the veins, but the majority of dolomite grows directly from the veins,
 235 and the portions of the host-rock away from the veins are generally undolomitized. This

236 kind of dolomitization is typically observed in the mudstone–wackestone beds of the
 237 Garbella Limestone.

238 Completely dolomitized rocks occur mainly in the Jurassic succession as discrete masses,
 239 some metres to some tens of metres wide, randomly distributed within partially dolomitized
 240 limestones. The two principal types are whitish, fine to medium crystalline dolostones and white,
 241 sucrosic, coarsely to very coarsely crystalline dolostones. Primary rock fabrics are commonly
 242 obliterated, although in some cases ghosts of the original fabric are still recognizable.

243

244 **Breccias**

245 Breccias form bodies with complex geometries, consisting of mainly tabular parts, at a high
 246 angle with respect to bedding, a few centimetres to some metres wide, which can be followed
 247 vertically for up to some tens of metres, and generally thinner bodies that develop along
 248 bedding planes in the host rock (Figs. 7, 11A and B). Four main breccia types have been
 249 recognized and are described below using the descriptive, non-genetic classification of
 250 carbonate breccias by Morrow (1982).

251- Type-1 are clast-supported, monomictic breccias with clasts of undolomitized rocks ,
 252 with the same lithology as the host rock. Clasts are generally angular and millimetre- to
 253 centimetre-sized and locally show a jigsaw-puzzle arrangement (Fig. 11C). Voids are
 254 cemented by millimetre- to centimetre-thick rims of white, coarsely to very coarsely
 255 crystalline dolomite, followed by calcite. Locally, internal sediments are present, either
 256 predating or postdating dolomite cements (Fig. 11D). Detailed petrographic and
 257 cathodoluminescence analyses show important differences and asymmetries in the
 258 stratigraphy of cement rims around different clasts or on different sides of the same
 259 clast. A gradual transition between veined limestones and type-1 breccias is commonly
 260 observed, occurring by a progressive increase of clast displacement resulting in the
 261 formation of centimetre-wide voids filled with coarse to very coarse dolomite cement
 262 (Fig. 11E). Clasts within these breccias are locally crossed by millimetre-thick dolomite
 263 veins and thus consist of veined limestones (Fig. 11F). Type-1 breccias can be either
 264 crackle, mosaic, or rubble packbreccias (sensu Morrow, 1982).

265- Type-2 are clast-supported, monomictic breccias with clasts of homogeneous, medium
 266 to coarsely crystalline dolostones, generally showing the same lithology as the host rock.
 267 They are centimetre- to decimetre-sized, and sub-rounded to angular in shape
 268 (Fig. 11G). Voids between the clasts are cemented by a millimetre- to centimetre-thick
 269 rim of coarsely to very coarsely crystalline white dolomite, with calcite plugging the

270 remaining pores. These breccias are mostly mosaic to rubble packbreccias or, less
 271 commonly, rubble floatbreccias (sensu Morrow, 1982).
 272- Type-3 are polymictic, clast-supported breccias with centimetre- to decimetre-sized,
 273 angular to subrounded clasts composed of coarsely-crystalline dolostones, limestones,
 274 and partially dolomitized limestones (including clasts of limestones with dolomite veins
 275 clearly truncated at the clast edge) (Fig. 11H). Voids between clasts are filled up with a
 276 micritic matrix containing sand-sized clasts of the same lithologies as larger clasts. Type-
 277 3 breccias are mostly rubble packbreccias (sensu Morrow, 1982).
 278- Type-4 are clast-supported monomictic breccias, mostly composed of millimetre- to
 279 centimetre-long and millimetre-wide plate-like clasts (rubble floatbreccias sensu Morrow,
 280 1982) (Fig. 12A). The clasts show a constant and particular fabric: a central part of finely
 281 to medium crystalline dolomite is surrounded on the two sides by coarse crystals of
 282 white dolomite growing outward from the central part. The shape of the clasts is angular,
 283 and their outline mostly coincides with the dolomite crystal faces. Voids between clasts
 284 are cemented by dark-grey, sparry calcite (Fig. 12A). Type-4 breccias are commonly
 285 found within veined limestone, as tabular bodies bordered by veins, forming a high angle
 286 with the host-rock bedding (Fig. 12B).

287

288Cavities

289Irregularly shaped cavities are frequent in the dolomitized rocks and are commonly millimetre- to
 290centimetre-sized, but they can locally reach several decimetres in diameter (Fig. 13A). Cavities
 291are commonly fringed by an isopachous rim of coarsely crystalline dolomite cement, locally
 292showing a jagged outline (Fig. 13B), followed by sparry calcite. They host internal sediments,
 293giving rise in some cases to geopetal structures (Fig. 13C). Sediments are mainly silt-sized,
 294locally passing to very fine and fine grained sands (up to 200 μm in diameter), and are
 295commonly laminated (Fig. 13D and E). They generally consist of calcite, but they locally contain
 296fragments of coarsely crystalline dolomite crystals. Laminae are some hundred micrometres to a
 297few millimetres in thickness and show a normal grading. Locally, these sediments are
 298dolomitized and appear as a homogeneous mosaic of anhedral to subhedral, finely to medium
 299crystalline dolomite crystals. In some large cavities, a first layer of dolomitized sediment is
 300followed by a second one of undolomitized sediment (Fig. 13E). In most cases internal
 301sediments are deposited above dolomite cement rims and are followed by calcite cement (Fig.
 30213C). Locally, however, sediments can occur in any position, from below the first cement
 303generation to above the last one.(e.g. Fig. 13D). Cavity fills also contain clasts which are

304 represented by fragments of the wall-rock or of early cement rims (Fig. 13A and E). A particular
 305 kind of cavities occurs in veined limestones and are entirely bordered by veins, giving rise to a
 306 boxwork fabric (Fig. 13F). A sparry calcite cement plugs these cavities.

307 Both partially and completely dolomitized rocks show a very low porosity, quantifiable as less
 308 than 2%. Cavities and fractures are completely occluded by cement, and no significant inter-
 309 crystalline porosity is present in dolostones.

310

311 **Reworked dolomite**

312 In the Colle di Tenda area, the Nummulitic Limestone directly overlies the dolomitized Garbella
 313 Limestone, and starts with a metre-thick bed of clast-supported conglomerate with decimetre-
 314 sized clasts of limestones and coarsely crystalline dolostones (Carraro *et al.*, 1970; Campredon,
 315 1977), with *Gastrochaenolites* bivalve borings (Fig. 14). The conglomerate is followed by a
 316 succession of decimetre-thick, normally graded beds, made up of conglomerates to arenites,
 317 whose clasts and grains consist of dolomitic rocks and fragments of single dolomite crystals with
 318 petrographic and cathodoluminescence features comparable to the underlying dolomitized
 319 carbonates. Similar dolostone clasts, have been recently found also in Cretaceous sediments of
 320 the adjoining Dauphinois succession, in particular in Valanginian–Hauterivian p.p. pebbly
 321 mudstones locally draping the Caire Porcera palaeomargin (Lausa Limestone; Barale, 2014;
 322 Barale *et al.*, 2016).

323

324 **PETROGRAPHY, CATHODOLUMINESCENCE, AND ELECTRON MICROSCOPY**

325 Petrographic analysis of the dolomitized rocks allowed different mineralogical phases related or
 326 subsequent to the dolomitization event to be distinguished. For dolomite phases, the
 327 morphological classification of Sibley and Gregg (1987) has been utilized. Four dolomite types
 328 have been recognized:

329- Dol1. Finely to medium crystalline planar-s dolomite. It has a turbid appearance in thin
 330 section due to the abundance of small fluid and solid inclusions. Dol1 occurs both as a
 331 cement in the inner parts of dolomite veins (Figs. 10D, E), and as replacement phase in
 332 all kinds of host limestones throughout the succession (Fig. 15A). Dol1 commonly gives
 333 rise to homogeneous, beige-coloured dolostones that do not preserve any relict primary
 334 depositional fabric. Dol1 shows a dull to moderate, blotchy, orange–red CL. This CL
 335 pattern invariably characterizes Dol1 throughout the study area.

336- Dol2. Coarsely to very coarsely crystalline planar-e dolomite. It occurs as a replacement
 337 phase, commonly in micritic facies of the Garbella Limestone, and forms euhedral

crystals, up to 1–2 mm in size (Fig. 15B), showing unit extinction under crossed polars. Crystals generally show a large inner portion with abundant micrometre-sized calcite inclusions representing portions of the replaced sediment and a clearer thin outer rim, some tens of micrometres thick, almost devoid of solid inclusions. Dol2 is commonly non-luminescent in CL. Only locally does the external part of the crystals have some hairline zones with moderate to bright red–orange CL.

Dol3. Non-planar, coarsely to extremely coarsely crystalline (500–5000 μm) dolomite. It has curved crystal faces and a marked sweeping extinction (Fig. 15C). In the outer part of the crystals, the alternation of more and less inclusion-rich bands defines a zoning which defines different growth stages. It occurs both as cement (saddle dolomite) and as replacive dolomite. The former gives rise to millimetre-thick rims fringing cavity walls and breccia clasts (Fig. 15B). Commonly, cavity-filling saddle dolomite has a cloudy inner part and a clear outer rim some tens of micrometres thick. Replacive Dol3 crystals typically grow from the veins outward (Fig. 10D and E) but also occur in the host limestone as isolated crystals, euhedral to subhedral and up to 2–3 mm in size. In some cases, Dol3 can completely replace the host rock, giving rise to a coarsely to very coarsely crystalline, sucrosic dolostone. In this case, it forms a mosaic of subhedral to anhedral crystals, 500–1000 μm in size on average, with larger crystals up to 4 mm in size. Larger crystals locally preserve ghosts of primary fabrics, evidenced by alignments of minute calcite inclusions. Dol3 crystals have, as a general trend, a thick inner part with a homogeneous, dull to moderate red–orange luminescence, analogous to that of Dol1. This zone is followed by a thick non-luminescent zone locally showing hairline, moderately to brightly luminescent orange zones. The outer part of the crystals has a moderate to bright luminescence with a well-defined zonation, resulting from the alternation of red–orange, orange, and non-luminescent zones (Fig. 16A and B).

Dol4. Fibrous dolomite cement, forming elongated, blade- to fan-shaped crystals with rhombic terminations, up to 7–8 mm long and 1–2 mm wide, with the long axis perpendicular to the substrate. Crystals show sweeping extinction with diverging optical axes of the fibres (fascicular-optic; e.g., Richter *et al.*, 2011) (Fig. 15D). Dol4 is common as breccia and cavity cement in the Mont Chajol sector, whereas it has not been observed in other sectors. Dol4 has a moderate orange or red–orange CL, with a well-defined zonation in the outer part of the crystals, deriving from the alternation of zones with slightly different CL colour or intensity.

372SEM–EDS analyses show that all the above-described phases are non-ferroan, high-Ca
373calcium dolomites (*sensu* Jones and Luth, 2002). The CaCO_3 content is 57–59 mol% in Dol1,
37454–56 mol% in Dol2, 56–59 mol% in Dol3, and 56–60 mol% in Dol4.

375Calcite (Cc1) represents the last phase of void cementation throughout the study area. It is a
376coarsely to extremely coarsely crystalline sparry calcite (Fig. 15C), forming anhedral crystals
377that commonly show polysynthetic twinning. It is generally limpid in thin section, whereas on the
378hand sample the colour is variable, from white to dark-grey or blackish (Fig. 13A and F); the
379latter smells like oil when crushed. Cc1 shows a dull to moderate yellow–orange to greenish
380yellow CL with a local zonation resulting from the alternation of luminescent and non-
381luminescent zones.

382Dol1, Dol3, and Cc1 are the most commonly observed phases and are widespread throughout
383the study area. Dol1 predates Dol3. This can be clearly observed in cavities, where Dol3 saddle
384dolomite cement grows on the Dol1 replacement dolomite commonly representing the cavity
385wall, and in veins, where the inner part, made up of Dol1, is overgrown by outward-growing Dol3
386crystals (Fig. 10D and E). Cc1 is the last phase of void filling, ubiquitously postdating Dol3
387cement. Dol2 has a wide distribution in the study area, but it seems to be limited to fine-grained
388host rocks (mudstones and wackestones), whereas Dol1 and Dol3 are common replacement
389phases in all types of rocks. Dol4 cement has only been observed in samples coming from the
390Mont Chajol sector.

391

392 **STABLE ISOTOPE GEOCHEMISTRY**

393Twenty dolomite samples were measured to determine their $\delta^{18}\text{O}$ and $\delta^{13}\text{C}$ isotopic values.
394Samples consisted of Dol1 replacement dolomite, Dol3 saddle dolomite cement, and Dol4
395cement. The data obtained are similar for all dolomite types (Fig. 17): $\delta^{18}\text{O}$ values range from –
3962.00 to –11.03‰ VPDB, and the majority of them range between –4 and –7‰ VPDB, whereas
397 $\delta^{13}\text{C}$ values mostly range between +1 and +2‰ VPDB. Two samples of Cc1 calcite were also
398measured: they show negative $\delta^{18}\text{O}$ values (–7.73 and –7.24‰ VPDB), whereas $\delta^{13}\text{C}$ values
399are –2.10 and +0.50‰ VPDB, respectively. Lastly, eight samples of undolomitized Triassic and
400Jurassic carbonates have been measured: they show $\delta^{18}\text{O}$ values between –4.21 and –1.63‰
401VPDB and $\delta^{13}\text{C}$ values between –0.53 and +2.53‰ VPDB.

402

403 **FLUID INCLUSION ANALYSIS**

404More than 100 fluid inclusions from 8 double-polished sections have been measured to find their
405homogenization temperatures with a standard heating method (Goldstein and Reynolds, 1994).

Primary fluid inclusions of useful size for microthermometry (i.e. greater than 2 μm in diameter; Goldstein and Reynolds, 1994) were found in the clear, outer rim of Dol3 and Dol4. The distribution of these inclusions along growth zones documents their primary origin. They are two-phase inclusions, liquid-rich with a vapour bubble, with irregular shapes, varying in size from 2–3 up to 10 μm . No evidence of stretching of either crystals or inclusions has been noted. Primary fluid inclusions show a relatively tight distribution of homogenization temperatures, ranging from 170 to 240 $^{\circ}\text{C}$ in Dol3 (highest frequency around 200 $^{\circ}\text{C}$) and from 190 to 260 $^{\circ}\text{C}$ in Dol4 (highest frequency around 230 $^{\circ}\text{C}$) (Fig. 18). Larger fluid inclusions in Dol3 were also utilized for low-temperature runs to infer the fluid composition. The only recognizable phase observed was ice, with final melting temperatures between -20 and -24 $^{\circ}\text{C}$, whereas the eutectic temperatures were not clearly determinable. The measured final melting temperatures of ice are lower than the eutectic temperature of the H_2O – NaCl system (-21.2 $^{\circ}\text{C}$), thus pointing to a more complex system with cations other than Na^+ , possibly Ca^{2+} and Mg^{2+} . Assuming a NaCl – CaCl_2 – MgCl_2 – H_2O system (eutectic temperature -57°C ; Shepherd *et al.*, 1985) as a possible approximation for the fluid inclusion composition, the observed final melting temperatures indicate a highly saline fluid with an approximate salinity of 20–23% CaCl_2 equivalent (salinity is expressed in CaCl_2 equivalent following Bakker and Baumgartner, 2012).

423

424 **DISCUSSION**

425

426 **Age of dolomitization**

On the basis of the stratigraphic relationships described in this paper, the timing of dolomite formation is well constrained. Dolomitization has to be younger than the youngest dolomitized rocks, which are the top interval of the Garbella Limestone, dated to the Berriasian. On the other hand, dolomitization has to be older than the oldest sediments containing dolomite clasts. Clasts derived from erosion of the dolomitized Garbella Limestone are present in Valanginian–Hauterivian p.p. sediments locally draping the Caire Porcera palaeomargin (Barale, 2014). The presence of dolostone clasts in Valanginian–Hauterivian p.p. sediments thus indicates that dolomitization cannot be younger than Valanginian. To summarize, the studied hydrothermal dolomitization occurred in the earliest Cretaceous, probably in the latest Berriasian–Valanginian interval.

437

438 **Burial conditions during dolomitization**

In order to reconstruct the diagenetic environment of dolomitization, the burial history of the host rocks has to be considered. As concluded above, dolomitization took place in the earliest Cretaceous (latest Berriasian–Valanginian). Lower Cretaceous sediments are very thin or completely missing in the study area, more likely due to condensation and non-deposition than to subsequent erosion. The Lower Cretaceous Provençal succession is in fact condensed throughout the Maritime Alps (e.g., Lanteaume, 1968, 1990; Decarlis & Lualdi, 2008; Barale *et al.*, 2013b). Thus, in the latest Berriasian–Valanginian, the top of the Garbella Limestone should have been very close to the seafloor. This is confirmed by the absence of compactional features (e.g., concave-convex grain contacts) in dolomitized ooid grainstone beds of the Garbella Limestone, documenting that dolomitization occurred before the onset of burial-related compaction of sediments (Fig. 10A). Moreover, in the Garbella Limestone, dolomite veins are locally cut by bedding-parallel stylolites, again indicating that dolomitization occurred before the deep burial of the succession (Fig. 9A).

Contextually, the lower part of the Middle Triassic carbonates should have been buried to a depth of 400–500 m, corresponding to the cumulative thickness of the Garbella Limestone and the Triassic carbonates themselves. For this reason, the temperature of the host rock at the time of the dolomitization event should have been very low, close to seawater temperature (which was around 35 °C at the surface in Early Cretaceous low-latitude seas: Schouten *et al.*, 2003, Littler *et al.*, 2011) in the upper part of the dolomitized succession and slightly higher in the lower part. On the other hand, microthermometric data indicate that dolomitizing fluids were significantly hotter (180–240 °C), and thus they can be properly considered as hydrothermal fluids (*sensu* Machel and Lonnee, 2002; Machel, 2004; Davies and Smith, 2006).

461

462 **Hydrothermal minerals**

Among the different mineral phases described above, Dol1, Dol2, and Dol3 dolomites and Cc1 calcite are the most important ones, as they are ubiquitous in the studied rocks. Dol4 is present only in a limited sector (Mont Chajol). Dol1 and Dol2 are both replacement phases, although showing very different features. It is not clear which factors controlled the development of Dol1 rather than Dol2. The host-rock lithology might have played some role, as Dol2 has been observed almost exclusively in micritic rocks whereas Dol1 replaces all kinds of host limestones. It is possible that partly lithified, and thus less porous and permeable, micritic host rock impeded an efficient flux of dolomitizing fluids thus allowing a smaller number of dolomite crystals to nucleate, and promoting their non-competitive growth to larger sizes, whereas in more porous host rocks, e.g. non-cemented carbonate sands, the competitive growth of numerous crystals

generally resulted in a small crystal size. Dol3 also occurs as a replacement phase. Comparable oxygen isotope values of Dol1 and Dol3, and the lack of fluid inclusion microthermometric data for Dol1, do not allow reliable hypotheses to be made on the factors controlling the development of Dol3 rather than Dol1.

Dol4 fascicular-optic dolomite is only present in the Mont Chajol area, where it forms thick cement rims in breccias, cavities, and veins, analogously to Dol3 saddle dolomite. Stable isotope and microthermometric data do not show clear differences between the fluids which precipitated Dol4 and those which precipitated Dol3 saddle dolomite, and thus do not allow us to understand which factors locally favoured the precipitation of Dol4 instead of Dol3.

Cc1 is the last phase of cement precipitation which plugs the remaining pores. Many examples are reported in which calcite is closely associated with dolomite as a late-stage hydrothermal phase precipitating at a lower temperature (e.g. Lavoie *et al.*, 2005; López-Horgue *et al.*, 2010; Sharp *et al.*, 2010). The change from dolomite to calcite precipitation has been related to a late-stage calcite saturation in the fluid as a result of Mg exhaustion or, alternatively, to a switch of hydrothermal fluids from dolomite to calcite supersaturation due to a drop in temperature.

488

489 **Rock fabrics**

The whole Middle Triassic to Berriasian succession, several hundreds of metres thick, is affected by dolomitization. Nevertheless, striking differences exist in the response of host rocks to the flow of dolomitizing fluids: in Triassic carbonates, breccias prevail and dolomitized bodies are smaller and scattered, whereas in the Middle Jurassic–Berriasian limestones a pervasive dolomitization (partial or complete) of the host limestones occurs (Fig. 3).

495

496 *Partial versus complete dolomitization*

Partially dolomitized rocks are volumetrically the most important form of dolomitization, and are affected by non-selective or selective dolomitization. The latter affects from place to place either the matrix or the grains, and seems to be controlled by a number of factors: crystal size of the calcareous precursor (micrite vs. monocrystalline echinoderm fragments), mineralogy of the calcareous precursor (aragonite vs. calcite), early diagenetic processes such as cementation and neomorphism modifying, respectively, permeability and chemical stability of grains (e.g., Murray and Lucia, 1967; Sibley, 1982; Bullen and Sibley, 1984; Sibley and Gregg, 1987). The features of the sediment resulting from either depositional or early diagenetic processes interplayed with the chemical characteristics of dolomitizing fluids (e.g., saturation) which, in

506turn, could vary both in space and time resulting in a complex spectrum of dolomitization
507modes.

508Veined limestones represent a common type of partially dolomitized rocks, and are commonly
509developed in mudstones or wackestones, whereas matrix-poor, grainy textures show a more
510diffuse dolomitization. Tight, partly litified, mud-supported sediments possibly did not allow a
511diffuse, pore-controlled, fluid flow, but only a focused flow through a network of fractures, and
512dolomite formation was limited to vein cement and substitution of the host rock adjacent to the
513vein walls. Completely dolomitized bodies are decimetre- to decametre-sized, show an irregular
514shape and are randomly distributed in the sedimentary succession and commonly discordant
515with the bedding. Only locally, in Middle Triassic carbonates, thin, laterally discontinuous, shale
516beds acted as minor barriers to the fluid flow and caused them to expand laterally, giving rise to
517decimetre- to metre-sized, stratabound dolomitized bodies. The factors controlling the
518distribution of dolomitized bodies probably lie in the intensity of the fluid flow and in the total
519volume of hydrothermal fluids circulating through the rock. These factors could be controlled in
520turn by the distance from the main fluid-flow pathways. Dolomitized bodies locally show a very
521sharp dolomitization front (Figs 6B, 8A and C), possibly corresponding to the margins of highly
522fractured rock volumes acting as fluid conduits.

523

524*Cavities*

525The irregular shapes of the cavities, generally with smooth and rounded edges, and their
526relatively large dimensions indicate that they formed as a consequence of dissolution
527processes. Moreover, the incongruent cement stratigraphy on different parts of cavity walls and
528around clasts, as well as the presence of cement clasts, indicate that cavity opening was a
529polyphase process. Phases of cavity enlargement by dissolution and subsequent cement
530precipitation on cavity walls likely alternated with phases of fracturing affecting both the cavity
531walls and the early cement rims grown on them (Figs. 11D, 13C, D and E, 19). Cavities
532commonly host laminated internal sediments. The relationships among the internal sediments
533and hydrothermal cements, in particular saddle dolomite, clearly document that the sediment
534deposition occurred indifferently before, after, or between different phases of cement
535precipitation (Fig. 19). This, together with the fact that internal sediments are locally dolomitized,
536indicates that sediment deposition occurred when the hydrothermal system was still active. As
537to the origin of the sediments, there are two possibilities. The first hypothesis is that sediments
538originated within the hydrothermal system, deriving both from the erosion of cavity and fracture
539walls during the flow of the hydrothermal fluids, and from mobilization of still unconsolidated

540 levels of the sedimentary succession. The second hypothesis, conversely, is that they derived
 541 from infiltration of loose sediment from the seafloor. Internal sediments are present both in
 542 cavities hosted in the Garbella Limestone, whose upper portion was close to the seafloor at the
 543 time of dolomitization, and in the Middle Triassic carbonates (Monte Chiamossero, Mont
 544 Agnelet), which during and after the dolomitization event were separated from the seafloor by
 545 the entire thickness of the Jurassic succession (over 200 m). This considerable depth value
 546 does not rule out, in principle, the possibility of a sediment infiltration from the seafloor. In fact,
 547 sediment infiltration has been documented in cavity networks down to a depth of 300 m from the
 548 seafloor (Aranburu *et al.*, 2002). However, internal sediments locally contain sand-sized
 549 dolomite clasts that have been recognized as fragments of cavity-wall cements. This indicates
 550 that at least a part of the sediments has an intra-system provenance, even though a mixing of
 551 intra- and extra-system sediments cannot be excluded.

552

553 *Breccias*

554 Breccias are characterized by some common features:

- 555- the angular shape and the jigsaw puzzle arrangement of clasts;
- 556- the apparent floating fabric of clasts, clearly due to dilation;
- 557- the high-angle orientation of the tabular breccia bodies with respect to host-rock
- 558 bedding.

559 These features point to hydrofracturing processes related to mainly vertical fluxes of
 560 overpressured fluids (e.g. Phillips, 1972; Ohle 1985). Most breccias are monomictic, with clasts
 561 of the same lithology as the encasing rock. This documents that they derive from in situ
 562 disruption of the encasing rock, with a limited or no transport at all of the clasts. Conversely, the
 563 polymictic nature of type-3 breccias implicates some sort of clast transport, even though it is not
 564 known over what distance. Also, the fine-grained matrix locally present in type-3 breccias likely
 565 derived from transport and deposition of loose sediments. As to the origin of these sediments,
 566 the same considerations as for internal sediments in cavities are valid. Rounded breccias clasts
 567 formed by partial dissolution of the clast edges (cf. Iannace *et al.*, 2012), as other rounding
 568 mechanisms, such as a prolonged transport, can be confidently ruled out.

569 Type-4 breccias deserve a separate discussion, because their unusual composition and fabric
 570 reflect a particular genetic mechanism. The shape and structure of the clasts strongly resemble
 571 those of the dolomite veins crosscutting the host limestones, and thus clasts reasonably
 572 represent fragments of such veins. Locally, on the outcrop, a lateral transition from veined
 573 limestones to type-4 breccias has been actually observed via a series of intermediate facies

574with increasing host-rock dissolution and disruption of the vein network. These breccias are
 575related to a dissolution process, locally affecting veined limestones. The steps of type-4 breccia
 576formation can be summarized as follows (Fig. 20):

- 577- The host limestone is crossed by a network of thin fractures. Dolomitizing fluids flow
- 578 through this crack system, resulting in dolomite cementation of the fractures and
- 579 dolomitization of their walls ;
- 580- a local but complete dissolution of the host limestone occurs, leaving a fragile network of
- 581 isolated dolomite veins (boxwork fabric);
- 582- the vein network collapses, forming clasts of vein material;
- 583- clasts are cemented by sparry calcite.

584In conclusion, type-1, -2, and -3 breccias originated through hydrofracturing processes and
 585show only local evidence of dissolution (rounded clasts). On the contrary, type-4 breccias are
 586only indirectly connected to hydrofracturing, but document strong dissolution of veined
 587limestones.

588

589**Characters and origin of dolomitizing fluids**

590The isotopic composition of hydrothermal dolomite shows slightly positive $\delta^{13}\text{C}$ values, mostly
 591between 1 and 2‰ VPDB, and negative $\delta^{18}\text{O}$ values, varying from -2 to -11‰ VPDB. The $\delta^{13}\text{C}$
 592values overlap with values from Triassic and Jurassic sediments not affected by hydrothermal
 593dolomitization and are in the range of carbonates precipitated from seawater (e.g. Podlaha *et*
 594*al.*, 1998; Nunn and Price 2010). This probably indicates that the host rock had a buffering effect
 595on the carbon-isotope composition of the dolomite, as is commonly observed in dolomitization
 596processes (e.g. Hoefs, 2009). Conversely, the $\delta^{18}\text{O}$ values of hydrothermal dolomite differ
 597significantly from the values of Triassic and Jurassic sediments not affected by hydrothermal
 598dolomitization, being markedly more negative. Calculation of the isotopic composition of the
 599parent fluids was made by combining the $\delta^{18}\text{O}$ data measured on hydrothermal dolomite with
 600the precipitation temperature obtained in the very same spots by fluid inclusion
 601microthermometry (this was possible in very coarse, Dol3 and Dol4 cements). According to the
 602fractionation equation of Land (1985), the combination of these data indicates highly ^{18}O -
 603enriched dolomitizing fluids, ranging from about +9 and +12‰ Standard Mean Ocean Water
 604(SMOW). The final melting temperature of fluid inclusions indicates that dolomitizing fluids were
 605highly saline fluids characterized by a complex composition that could be represented by the
 606NaCl–CaCl₂–MgCl₂–H₂O system and an approximate salinity of 20–23% CaCl₂ equivalent.
 607Basinal and evaporitic brines are commonly indicated as probable sources of highly saline fluids

in hydrothermal systems (e.g. Davies and Smith, 2006; López-Horgue *et al.*, 2010; Shah *et al.*, 2012; Laponi *et al.*, 2014). Moreover, such brines are highly ^{18}O -enriched, as are waters deriving from salt dissolution or gypsum dehydration (Hitchon and Friedman, 1969; Knauth and Beeunas, 1986). In the study area, basinal brines could have entered the hydrothermal system only from the adjoining Dauphinois succession, that, however, was too thin (a few hundred metres; Carraro *et al.*, 1970; Barale *et al.*, 2016) to provide large amounts of fluids. For this reason, the most important source of fluids was likely to be seawater, whose original composition still had to be strongly modified to produce the highly saline, ^{18}O -enriched dolomitizing fluids. The interaction with evaporite intervals is commonly invoked to explain the high salinity and $\delta^{18}\text{O}$ values of dolomitizing fluids (e.g. López-Horgue *et al.*, 2010; Shah *et al.*, 2012; Laponi *et al.*, 2014; Geske *et al.*, 2015). Upper Triassic evaporites are present in the stratigraphic succession of the Maritime Alps (Lanteaume, 1968; Carraro *et al.*, 1970). This evaporite interval represents a preferential detachment horizon in the stratigraphic succession and it is not cropping out at present in the study area due to tectonic lamination, even though masses of Upper Triassic evaporites are locally present in the subsurface (Colle di Tenda tunnel; Ivaldi *et al.*, 1998; Cavinato *et al.*, 2006). However, the original thickness of Upper Triassic evaporites is unknown, and therefore it is not possible to establish if this interval could have played a significative role in modifying the composition of dolomitizing fluids. Another possible mechanism for increasing the salinity of fluids and enriching them in ^{18}O is the interaction with silicate minerals of siliciclastic and crystalline rocks (Clayton *et al.*, 1966; Land and Prezbindowski, 1981; Hitchon *et al.*, 1990). As mentioned above, high precipitation temperatures document that dolomitizing fluids were involved in a deep hydrothermal circulation. Considering the extreme reduction of the Middle Triassic–Jurassic sedimentary succession in this area (not more than 400–500 m), it is very likely that fluids interacted with Permian–Lower Triassic siliciclastic rocks and with the crystalline rocks of the basement, currently exposed in the Argentera Massif (Fig. 21). This interaction possibly accounts for the enrichment in ^{18}O and the increase in salinity of the dolomitizing fluids. Actually, the less ^{18}O -enriched values of the dolomitizing fluids, calculated from the most ^{18}O -depleted dolomites, can be considered as the most representative of the fluids. The less depleted values of the dolomite could conversely be the result of important interactions between dolomitizing fluids and host rocks and as such not suitable to calculate the isotopic composition of dolomitizing fluids. A reasonable value for the latter therefore is around +8‰ SMOW or even lower and hence perfectly consistent with waters that have strongly interacted with silicate-rich basement rocks (e.g., Haeri-Ardakani *et al.*, 2013a, b).

642

643 **Processes and features of the hydrothermal system**

644 Temperatures obtained for dolomitizing fluids are anomalously high if compared to the low
 645 temperatures inferred for the dolomitized rocks from their shallow burial depth. In the study area
 646 there is no evidence of magmatic activity in the Mesozoic, which could have represented a heat
 647 source for the fluids. Therefore, the high temperature of the fluids documents a very deep
 648 hydrothermal circulation related to deep-rooted fault systems (Fig. 21)., as commonly
 649 hypothesized for hydrothermal systems related to high-temperature and shallow-burial
 650 dolomitization (e.g. Davies and Smith, 2006; López-Horgue *et al.*, 2010; Shah *et al.*, 2012).
 651 In the study case, the measured homogenization temperatures of around 200° C would imply,
 652 assuming a normal geothermal gradient of about 30 °C/km, a circulation depth of at least 7 km.
 653 However, in extensional continental margins, crustal thinning is associated with anomalously
 654 high geothermal gradients (up to 80 °C/Km; Goldberg and Leyreloup, 1990; Vacherat *et al.*,
 655 2014), which moreover can persist for a few tens of Myr after the end of rifting (Vacherat *et al.*,
 656 2014). Such high gradients would significantly reduce the maximum depth of the hydrothermal
 657 system. The ubiquitous association of dolomitized bodies with vein networks and the common
 658 presence of dolomite-cemented, subvertical, tabular breccia bodies indicate that dolomitization
 659 was related to the circulation of fluids through high-angle faults and the related fracture systems.
 660 In this sense, the hydrothermal system was controlled by fracture porosity (*sensu* Choquette
 661 and Pray, 1970) related to faults and fracture systems, which exerted the most important control
 662 on the permeability of the host carbonates (e.g. Iriarte *et al.*, 2012). Intrinsic porosity variations
 663 among the different rock facies had only a minor control on fluid circulation, possibly influencing
 664 the distribution of dolomitization only at the very local scale and away from the major fluid-flow
 665 pathways, where the fluid flow was less intense and pervasive. Dolomite both precipitated along
 666 fault and fracture systems and replaced, partially or completely, non-fractured portions of
 667 carbonate rocks. This indicates that part of the host carbonates were still permeable enough to
 668 allow a diffuse flux of dolomitizing fluids. At the time of dolomitization, the Triassic and Jurassic
 669 parts of the succession differed in several aspects, such as lithofacies, composition,
 670 permeability, coherence, and burial depth, which altogether influenced the modes of
 671 dolomitization. The Triassic sediments were mainly fine-grained limestones and dolostones, and
 672 evenly bedded because of thin shale partings. Moreover, their porosity was reduced by the
 673 overburden of the overlying sediment column. Therefore, on the whole, they were less
 674 permeable and compositionally less prone to dolomite replacement. Conversely, the Jurassic
 675 succession was more shallowly buried and in part composed of coarse-grained, mud-poor

676carbonate sediments. Consequently, pervasive dolomitization was favoured in the more
677permeable and shallower Jurassic limestones, whereas deeper in the rock column, hydraulic
678fracturing processes prevailed with the development of a network of breccia conduits.
679The random 3D orientation of vein networks and the common presence of hydrofracturing-
680related breccias indicate the importance of hydrofracturing processes in the evolution of the
681hydrothermal system. Hydrofracturing was related to the abrupt expulsion of overpressured
682fluids along main fluid-flow pathways, likely represented by high-angle faults and the related
683subvertical breccia bodies and fracture systems. Polyphase breccias point to multiple events of
684hydrofracturing, in turn related to cyclic expulsion of overpressured fluids. Cyclic fluid expulsion
685through fault systems can be explained by the so-called fault–valve model (Ramsay, 1980;
686Sibson, 1987, 1992), which involves alternating phases of fluid accumulation and expulsion. It is
687thus probable that events of fault activity coincided with periods of hydrothermal activity, causing
688extensive hydrofracturing phenomena followed by massive fluid expulsion through the just
689opened fracture systems.

690The circulation of hydrothermal fluids had the dual effect of causing the replacive dolomitization
691of the host rock, and the precipitation of dolomite cements in fractures, among breccia clasts
692and in other voids. The solubility of dolomite is controlled by several parameters, including
693temperature, pH, partial pressure of CO₂, and concentration of carbonate and other ions in the
694fluid. In hydrothermal systems, however, the decrease of the fluid pressure is the process most
695commonly invoked to explain fluid supersaturation and dolomite precipitation (e.g. Davies and
696Smith, 2006; Swennen *et al.*, 2012). According to the above-cited fault–valve model, the abrupt
697release of overpressured fluids and their expulsion through fracture systems result in a
698significant pressure decrease. This caused a reduction of the partial pressure of CO₂ and thus
699an increase of the fluid saturation with respect to dolomite.

700Different features, including dissolution cavities, type-4 breccias, and rounded breccia clasts,
701indicate that the hydrothermal system was also punctuated by limestone dissolution episodes.
702Calcite dissolution in hydrothermal systems is commonly attributed to a decrease of fluid
703temperature, because calcite solubility increases as temperature decreases (hydrothermal karst
704effect; Giles and de Boer, 1990). Rounded dolostone breccia clasts are the unique feature
705pointing to large-scale dissolution of dolomite (cf. Sharp *et al.*, 2010). Nonetheless this is not
706conclusive evidence, as dissolution could also have affected the clasts before their
707dolomitization, when they were still composed of limestone. Good evidence of dolomite
708dissolution indeed exists albeit at a much smaller scale. The jagged outline of Dol3 saddle

709dolomite crystals, rimming cavities (Fig. 13B), points to the flow of aggressive fluids that resulted
710in the corrosion of the exposed dolomite cement crystals.

711

712REGIONAL CONTEXT

713In the classical Alpine literature, the Dauphinois–Provençal Domain has always been
714considered the proximal portion of the European continental margin (e.g. Debelmas and
715Lemoine, 1970; Debelmas and Kerckhove, 1980; Stämpfli and Marthaler, 1990), separated
716during the Late Triassic–Early Jurassic rifting phase of the Western Alpine Tethys, which finally
717led to the opening of the Ligurian–Piemonte ocean in the Bajocian (Bill *et al.*, 2001). The
718recognition of an Early Cretaceous hydrothermal dolomitization in the Provençal Domain
719provides a robust, although indirect, evidence of Early Cretaceous, post-rift tectonics in this
720sector of the European palaeomargin. As discussed above, the inferred temperature of the
721hydrothermal fluids and the large volumes of the rock bodies affected by dolomitization point to
722a huge and very deep hydrothermal system, in turn related to deep-rooted faults which could
723correspond to a segment of the proto-Periadriatic transform system (*sensu* Handy *et al.*, 2010;
724Fig. 22). This important E–W-trending transform fault was active since the Bajocian,
725accommodating differential spreading of the Piemonte and Ligurian oceans. It continued its
726activity in the Middle–Late Jurassic and in the Early Cretaceous, when it was possibly
727connected to the Iberia–Europe plate boundary, which acted as a lithosphere-scale, left-lateral
728strike-slip fault. This strike-slip activity continued at least until the Aptian–Albian, when a
729regional plate kinematic reorganization caused the divergence between Europe and Iberia and
730the onset of oceanic spreading in the Bay of Biscay (Tugend *et al.*, 2015, and reference
731therein).

732Extensional to strike-slip tectonics was active at least until the Aptian, and is documented both
733in the External Briançonnais Domain (Bertok *et al.*, 2012) and in the present French subalpine
734domain, where it controlled the evolution of the boundary between the Provençal platform and
735the Dauphinois basin (e.g. Dardeau and de Graciansky, 1987; de Graciansky and Lemoine,
7361988; Hibschi *et al.*, 1992; Montenat *et al.*, 1997, 2004; Friès and Parize, 2003; Masse *et al.*,
7372009).

738

739CONCLUSIONS

740Detailed field, petrographic, and geochemical analysis, as well as fluid inclusion
741microthermometry, allowed a comprehensive characterization of the hydrothermal dolomitization

largely affecting the Mesozoic Provençal carbonates in the French-Italian Maritime Alps. The main features of this process can be summarized as follows:

744

745- Dolomitization was a polyphase process, strictly associated with hydrofracturing events.
 746 Hydraulic fracturing was a consequence of the abrupt expulsion of overpressured fluids
 747 along main fluid-flow pathways, likely represented by high-angle faults and the related
 748 fracture systems. Circulation of hydrothermal fluids caused both replacive dolomitization
 749 of the host rock and dolomite cementation of fractures, breccias, and voids.

750

751- Dolomitizing fluids were hot (170–260 °C), highly saline, and ¹⁸O-enriched brines, likely
 752 derived from modification of seawater due to rock–fluid interactions with sedimentary as
 753 well as crystalline basement rocks during hydrothermal circulation.

754

755- Dolomitization occurred in the earliest Cretaceous, when the Provençal carbonates were
 756 at a very shallow burial depth (from a few tens of metres to about 500 m). Therefore, the
 757 high temperature of the fluids documents a very deep hydrothermal circulation related to
 758 deep-rooted fault systems which represented the local physical expression of major
 759 changes in the tectonic regime of the Western Alpine Tethys.

760

761The study case represents a striking example of fossil hydrothermal system where high-
 762temperature, deep-circulating fluids lead to the dolomitization of huge volumes of carbonate
 763rocks at unusually shallow burial depth (< 500 m). The recognition of such evidence in an Alpine
 764setting is particularly significant since it provides a good, although indirect, evidence of pre-
 765orogenic tectonic activity in areas where successive collisional tectonics mostly overprinted the
 766ancient faults.

767

768

769ACKNOWLEDGEMENTS

770The authors thank the Associate Editor Cathy Hollis, the reviewers Alessandro Iannace and
 771Mikel A. López-Horgue, and an anonymous reviewer, whose useful suggestions and
 772constructive criticisms really improved the manuscript. Stefano Bernasconi and Maria Isabel
 773Millán (ETH Geological Institute, Zurich) are kindly acknowledged for realization of C and O
 774isotope analyses, and Simona Ferrando (Dipartimento di Scienze della Terra, Università di
 775Torino) for guidance and assistance in fluid inclusion microthermometry. The research was

supported by the University of Torino (ex 60% funds; Doctoral School of Sciences and Innovative Technologies funds) and by the Italian CNR (National Research Council), Istituto di Geoscienze e Georisorse, unità di Torino. Funds related to the ProGeoPiemonte Project (financed by Compagnia di San Paolo and University of Torino) have also been utilized. A financial contribution by the Italian Association for Sedimentary Geology (GeoSed) (Contributo Giovani 2011 to L. Barale) is gratefully acknowledged.

REFERENCES

- Aranburu, A., Fernández-Mendiola, P.A., López-Horgue, M.A. and García-Mondéjar, J.** (2002) Syntectonic hydrothermal calcite in a faulted carbonate platform margin (Albian of Jorrios, northern Spain). *Sedimentology*, **49**, 875–890.
- Bakker, R.J. and Baumgartner, M.** (2012) Unexpected phase assemblages in inclusions with ternary H₂O–salt fluids at low temperatures. *Centr. Eur. J. Geosci.*, **4**, 225–237.
- Barale, L.** (2014) The Meso–Cenozoic stratigraphic successions adjoining the Argentera Massif: stratigraphic, sedimentologic and diagenetic evidence of syndepositional tectonics. Unpubl. PhD Thesis, Università di Torino, 240 pp.
- Barale, L., Bertok, C., d’Atri, A., Domini, G., Martire, L. and Piana, F.** (2013a) Hydrothermal dolomitization of the carbonate Jurassic succession in the Provençal and Subbriançonnais Domains (Maritime Alps, North-Western Italy). *Comptes-Rendus Geoscience*, **345**, 47–53.
- Barale, L., d’Atri, A. and Martire, L.** (2013b) The role of microbial activity in the generation of Lower Cretaceous mixed Fe-oxide–phosphate ooids from the Provençal Domain, French Maritime Alps. *J. Sed. Res.*, **83**, 196–206.
- Barale, L., Bertok, C., d’Atri, A., Martire, L., Piana, F. and Domini, G.** (2016) Geology of the Entracque–Colle di Tenda area (Maritime Alps, NW Italy). *Journal of Maps*, **12**, 359–370. DOI: 10.1080/17445647.2015.1024293
- Bersezio, R. and d’Atri, A.** (1986) Nota preliminare sulla stratigrafia del Trias medio della copertura sedimentaria del massiccio dell’Argentera nell’alta Valle Roja. *Atti Acc. Naz. Lincei*, **80**, 135–144.
- Bertok, C., Martire, L., Perotti, E., d’Atri, A. and Piana, F.** (2012) Kilometre-scale palaeoescarpments as evidence for Cretaceous synsedimentary tectonics in the External Briançonnais domain (Ligurian Alps, Italy). *Sediment. Geol.*, **251**, 58–75.

- 808 **Bigot, M., Damiani, L., Dellery, B. and Durozoy, G.** (1967) Notice explicative, Carte
 809 Géologique de la France à 1:50.000, feuille Saint-Martin-Vésubie–Le Boréon. BRGM, Orléans,
 810 29 pp.
- 811 **Bill, M., O'Dogherty, L., Guex, J., Baumgartner, P. O. and Masson, H.** (2001). Radiolarite
 812 ages in Alpine-Mediterranean ophiolites: Constraints on the oceanic spreading and the Tethys–
 813 Atlantic connection. *GSA Bull.*, **113**, 129–143.
- 814 **Boni, M., Parente, G., Bechstädt, T., De Vivo, B. and Iannace, A.** (2000) Hydrothermal
 815 dolomites in SW Sardinia (Italy): evidence for a widespread late-Variscan fluid flow event.
 816 *Sediment. Geol.*, **131**, 181–200.
- 817 **Breitenbach, S.F.M. and Bernasconi, S.M.** (2011) Carbon and oxygen isotope analysis of
 818 small carbonate samples (20 to 100 µg) with a GasBench II preparation device. *Rapid Commun.*
 819 *Mass Spectrom.*, **25**, 1910–1914.
- 820 **Bullen, S.R. and Sibley, D.F.** (1984) Dolomite selectivity and mimic replacement. *Geology*, **12**,
 821 655–658.
- 822 **Campanino Sturani, F.** (1967) Sur quelques Nérinées du Malm des Alpes Maritimes
 823 (couverture sédimentaire de l'Argentera et écaïlles charriées du Col de Tende). *Rendiconti Acc.*
 824 *Naz. Lincei*, **42**, 527–529.
- 825 **Campredon, R.** (1977) Les Formations Paléogènes des Alpes-Maritimes franco–italiennes.
 826 *Mém. H.S. Soc. Géol. France*, **9**, 1–199.
- 827 **Carmichael, S.K. and Ferry, J.M.** (2008) Formation of replacement dolomite in the Latemar
 828 carbonate buildup, Dolomites, Northern Italy: part2. Origin of the dolomitizing fluid and the
 829 amount and duration of fluid flow. *Am. J. Sci.*, **308**, 885–904.
- 830 **Carmichael, S.K., Ferry, J.M., and McDonough, W.F.** (2008) Formation of replacement
 831 dolomite in the Latemar carbonate buildup, Dolomites, Northern Italy: part1. Field relations,
 832 mineralogy and geochemistry. *Am. J. Sci.*, **308**, 851–884.
- 833 **Carraro, F., Dal Piaz, G.V., Franceschetti, B., Malaroda, R., Sturani, C. and Zanella, E.**
 834 (1970) Note Illustrative della Carta Geologica del Massiccio dell'Argentera alla scala 1: 50.000.
 835 *Mem. Soc. Geol. Ital.*, **9**, 557–663.
- 836 **Cavinato, G.P., Di Luzio, E., Moscatelli, M., Vallone, R., Averardi, M., Valente, A. and**
 837 **Papale, S.** (2006) The new Col di Tenda tunnel between Italy and France: Integrated geological
 838 investigations and geophysical prospections for preliminary studies on the Italian side. *Engin.*
 839 *Geol.*, **88**, 90–109.
- 840 **Clayton, R.N., Friedman, I., Graf, D.L., Mayeda, T.K., Meents, W.F. and Shimp, N.F.** (1966)
 841 The origin of saline formation waters: I. Isotopic composition. *J. Geophys. Res.*, **71**, 3869–3882.

- 842**Costamagna, L.** (2013) Middle Triassic carbonate lithostratigraphy of the Southern
843Briançonnais (Cottian Alps, Italy) and comparison with the surrounding areas. *GeoActa*, **12**, 1–
84424.
- 845**Dardeau, G.** and **Bulard, P.F.** (1978) Répartition des dolomies du Jurassique supérieur de l'Arc
846de Nice (Alpes-Maritimes). *Bull. B.R.G.M.*, **2**, 79–88.
- 847**Dardeau, G.** and **de Graciansky, P.C.** (1987) Indices d'une tectonique synsédimentaire d'âge
848crétacé inférieur dans la basse vallée de l'Esteron (Alpes-Maritimes) et conséquences
849géodynamiques. *Bull. Soc. Géol. Fr.*, **3**, 1207–1210.
- 850**d'Atri, A., Piana, F., Barale, L., Bertok, C.** and **Martire, L.** (2016) Geological setting of the
851southern termination of Western Alps. *Int. J. Earth Sci.*, DOI: 10.1007/s00531-015-1277-91
- 852**Davies, G.R.** and **Smith, L.B. Jr.** (2006) Structurally controlled hydrothermal dolomite reservoir
853facies: An overview. *AAPG Bull.*, **90**, 1641–1690.
- 854**Debelmas, J.** and **Lemoine, M.** (1970) The Western Alps: paleogeography and structure.
855*Earth-Sci. Rev.*, **6**, 221–256.
- 856**Debelmas, J.** and **Kerckhove, C.** (1980) Les Alpes franco-italiennes. *Géol. Alp.*, **56**, 21–58.
- 857**Decarlis, A.** and **Lualdi, A.** (2008) Stratigraphy and deposition of lower Cretaceous condensed
858deposits in the Maritime Alps (Nice arc, SE France). *It. J. Geosci.*, **127**, 13–24.
- 859**de Graciansky, P.C.** and **Lemoine, M.** (1988) Early Cretaceous extensional tectonics in the
860southwestern French Alps: a consequence of North-atlantic rifting during Tethyan spreading.
861*Bull. Soc. Géol. Fr.*, **4**, 733–737.
- 862**Dumont, T., Schwartz, S., Guillot, S., Simon-Labric, T., Tricart, P.** and **Jourdan, S.** (2012)
863Structural and sedimentary records of the Oligocene revolution in the Western Alpine arc. *J.*
864*Geodyn.*, **56–57**, 18–38.
- 865**Faure-Muret, A.** (1955) Etudes géologiques sur le massif de l'Argentera–Mercantour et ses
866enveloppes sédimentaires. *Mém. Carte Géol. France*, Paris, 336 pp.
- 867**Faure-Muret, A., Fallot P.** and **Lanteaume M.** (1967) Carte Géologique de la France à
8681:50.000, feuille St-Martin-Vésubie–Le Boréon (947). Bureau de Recherches Géologiques et
869Minières, Orléans.
- 870**Ferry, J.M., Passey, B.H., Vasconcelos, C.** and **Eiler, J.M.** (2011) Formation of dolomite at
87140–80 °C in the Latemar carbonate buildup, Dolomites, Italy, from clumped isotope
872thermometry. *Geology*, **39**, 571–574.
- 873**Folk, R.L.** (1962) Spectral subdivision of limestone types. In: *Classification of Carbonate Rocks*.
874(Ed. W.E. Ham), AAPG, Tulsa, 62–84.

- 875 **Friès, G. and Parize, O.** (2003) Anatomy of ancient passive margin slope systems: Aptian
876 gravity-driven deposition on the Vocontian palaeomargin, western Alps, south-east France.
877 *Sedimentology*, **50**, 1231–1270.
- 878 **Geske, A., Goldstein, R.H., Mavromatis, V., Richter, D-K., Buhl, D., Kluge, T., John, C.M.**
879 and **Immenhauser, A.** (2015) The magnesium isotope ($\delta^{26}\text{Mg}$) signatures of dolomites.
880 *Geochimica et Cosmochimica acta*, **149**, 131–151.
- 881 **Giles, M.R. and De Boer, R.B.** (1990) Origin and significance of redistributive secondary
882 porosity. *Mar. Petrol. Geol.*, **7**, 379–397.
- 883 **Goldberg, J.M. and Leyreloup, A.F.** (1990) High temperature–low pressure Cretaceous
884 metamorphism related to crustal thinning (eastern North-Pyrenean zone, France). *Contrib.*
885 *Mineral. Petr.*, **104**, 194–207.
- 886 **Goldstein, R.H. and Reynolds, T.J.** (1994) Systematics of Fluid Inclusions in Diagenetic
887 Minerals. SEPM Short Course 31, Tulsa, 199 pp.
- 888 **Guo, X., He, S., Liu, K., Cao, F., Shi, H. and Zhu, J.** (2011) Condensates in the PY30-1
889 structure, Panyu Uplift, Pearl River Mouth Basin, South China Sea: evidence for hydrothermal
890 activity associated with petroleum migration and accumulation. *J. Petr. Geol.*, **34**, 217–232.
- 891 **Handy, M. R., Schmid, S. M. , Bousquet, R. , Kissling, E. and Bernoulli, D.** (2010)
892 Reconciling plate-tectonic reconstructions of Alpine Tethys with the geological-geophysical
893 record of spreading and subduction in the Alps. *Earth Sci. Rev.*, **102**, 3–4, 121–158.
- 894 **Haeri-Ardakani, O., Al-Aasm, I. and Coniglio, M.** (2013a) Fracture mineralization and fluid
895 flow evolution: an example from Ordovician–Devonian carbonates, southwestern Ontario,
896 Canada. *Geofluids*, **13**, 1–20.
- 897 **Haeri-Ardakani, O., Al-Aasm, I. and Coniglio, M.** (2013b) Petrologic and geochemical
898 attributes of fracture-related dolomitization in Ordovician carbonates and their spatial distribution
899 in southwestern Ontario, Canada. *Mar. Petrol. Geol.*, **43**, 409–422.
- 900 **Hendry, J.P., Gregg, J.M., Shelton, K.L., Somerville, I.D. and Crowley, S.F.** (2015) Origin,
901 characteristics and distribution of fault-related and fracture-related dolomitization: Insights from
902 Mississippian carbonates, Isle of Man. *Sedimentology*, **62**, 717–752.
- 903 **Hewett, D.F.** (1928) Dolomitization and ore deposition. *Econ. Geol.*, **23**, 821–863.
- 904 **Hibsch, C., Jandel, D., Montenat, C. and Ott d’Estevou, P.** (1992) Événements tectoniques
905 crétacés dans la partie méridionale du bassin subalpin (massif Ventoux–Lure et partie orientale
906 de l’arc de Castellane, SE France). Implications géodynamiques. *Bull. Soc. Géol. France*, **163**,
907 147–158.

- 908 **Hitchon, B.** and **Friedman, L.** (1969) Geochemistry and origin of formation waters in the
 909 western Canadian sedimentary basin. I. Stable isotopes of hydrogen and oxygen. *Geochim.*
 910 *Cosmochim. Ac.*, **33**, 1321–1349.
- 911 **Hitchon, B., Bachu, S.** and **Underschulz, J.R.** (1990) Regional subsurface hydrogeology,
 912 Peace River arch area, Alberta and British Columbia. *Bull. Can. Petrol. Geol.*, **38**, 196–217.
- 913 **Hoefs J.** (2009) Stable Isotope Geochemistry. 6th Edition. Springer-Verlag, Berlin–Heidelberg,
 914 285 pp.
- 915 **Iannace, A., Gasparini, M., Gabellone, T.** and **Mazzoli, S.** (2012) Late dolomitization in
 916 basinal limestones of the Southern Apennines fold and thrust belt (Italy). *Oil Gas Sci. Technol.*,
 917 **67**, 59–75.
- 918 **Iriarte, E., López-Horgue, M.A., Schroeder, S.** and **Caline, B.** (2012) Interplay between
 919 fracturing and hydrothermal fluid flow in the Asón Valley hydrothermal dolomites (Basque–
 920 Cantabrian Basin, Spain). In: *Advances in carbonate exploration and reservoir analysis* (Eds. J.
 921 Garland, J.E. Neilson, S.E. Laubach and K.J. Whidden), *Geol. Soc. London, Sp. Pub.*, **370**, 207–
 922 227.
- 923 **Ivaldi, J.-P., Guardia, P., Barbé, J.-F., Calvino, A., Meneroud, J.-P.** and **Richard, J.-C.** (1998)
 924 Mobilité crustale et diapirisme actif depuis le Crétacé au col de Tende, dans les Alpes maritimes
 925 franco–italiennes. *C.R. Acad. Sci. Paris, Earth Plan. Sci.*, **326**, 655–662.
- 926 **Jones, B.** and **Luth, R.W.** (2002) Dolostones from Grand Cayman, British West Indies. *J. Sed.*
 927 *Res.*, **72**, 559–569.
- 928 **Knauth, L.P.** and **Beeunas, M.A.** (1986) Isotope geochemistry of fluid inclusions in Permian
 929 halite with implications for the isotopic history of ocean water and origin of saline formation
 930 waters. *Geochim. Cosmochim. Ac.*, **50**, 419–433.
- 931 **Land, L.S.** (1985) The origin of massive dolomite. *J. Geol. Educ.*, **33**, 112–125.
- 932 **Land, L.S.** and **Prezbindowski, D.R.** (1981) The origin and evolution of saline formation
 933 waters, Lower Cretaceous carbonates, south–central Texas and southern New Mexico. *J.*
 934 *Hydrogeol.*, **54**, 51–74.
- 935 **Lanteaume, M.** (1968) Contribution à l'étude géologique des Alpes Maritimes franco–italiennes.
 936 *Mém. Carte Géol. France*, Paris, 405 pp.
- 937 **Lanteaume M.** (1990) Carte Géologique de la France à 1:50.000, feuille Vieve–Tende (948).
 938 Bureau de Recherches Géologiques et Minières, Orléans.
- 939 **Lapponi, F., Bakker, R.J.** and **Bechstædt, T.** (2007) Low temperature behaviour of natural
 940 saline fluid inclusions in saddle dolomite (Paleozoic, NW Spain). *Terra Nova*, **19**, 440–444.

- 941 **Lapponi, F., Bechstædt, T., Boni, M., Banks, D.A. and Schneider, J.** (2014) Hydrothermal
 942 dolomitization in a complex geodynamic setting (Lower Palaeozoic, northern Spain).
 943 *Sedimentology*, **61**, 411–443.
- 944 **Lavoie, D., Chi, G., Brennan-Alpert, P., Desrochers, A. and Bertrand, R.** (2005)
 945 Hydrothermal dolomitization in the Lower Ordovician Romaine Formation of the Anticosti Basin:
 946 significance for hydrocarbon exploration. *Bull. Can. Petrol. Geol.*, **53**, 454–471.
- 947 **Little, K., Robinson, S.A., Bown, P.R., Nederbragt, A.J. and Pancost, R.D.** (2011) High sea-
 948 surface temperatures during the Early Cretaceous Epoch. *Nature*, **4**, 169–172.
- 949 **López-Horgue, M.A., Iriarte, E., Schröeder, S., Fernández-Mendiola, P.A., Caline, B.,**
 950 **Corneillie, H., Frémont, J., Sudrie, M. and Zerti, S.** (2010) Structurally controlled
 951 hydrothermal dolomites in Albian carbonates of the Asón valley, Basque Cantabrian Basin,
 952 Northern Spain. *Mar. Petrol. Geol.*, **27**, 1069–1092.
- 953 **Machel, H.G.** (2004) Concepts and models of dolomitization: a critical reappraisal. In: *The*
 954 *Geometry and Petrogenesis of Dolomite Hydrocarbon Reservoirs* (Eds. C.J.R. Braithwaite, G.
 955 Rizzi and G. Darke), *Geol. Soc. London, Sp. Pub.*, 235, 7–63.
- 956 **Machel, H.G. and Lonnee, J.** (2002) Hydrothermal dolomite – a product of poor definition and
 957 imagination. *Sediment. Geol.*, **152**, 163–171.
- 958 **Malaroda, R.** (Ed.) (1970) Carta Geologica del Massiccio dell'Argentera alla scala 1:50.000.
 959 *Mem. Soc. Geol. Ital.*, **9**.
- 960 **Malaroda, R.** (1999) L'Argentera meridionale – Memoria illustrativa della “Geological Map of
 961 Southern Argentera Massif (Maritime Alps) 1 :25 000”. *Mem. Sci. Geol.*, **51–52**, 241–331.
- 962 **Masse, J.-P., Villeneuve, M., Leonforte, E.-and Nizou, J.** (2009) Block tilting of the North
 963 Provence early Cretaceous carbonate margin: stratigraphic, sedimentologic and tectonic data.
 964 *Bull. Soc. Géol. France*, **180**, 105–115.
- 965 **McCrea, J.M.** (1950) On the isotopic chemistry of carbonates and paleotemperature scale. *J.*
 966 *Chem. Phys.*, **18**, 849–857.
- 967 **Montenat, C., Hirsch, C., Perrier, J.C., Pascaud, F. and De Bretizel, P.** (1997) Tectonique
 968 cassante d'âge crétacé inférieur dans l'Arc de Nice (Alpes-Maritimes, France). *Géol. Alp.*, **73**,
 969 59–66.
- 970 **Montenat, C., Janin, M.-C. and Barrier, P.** (2004) L'accident du Toulourenc: une limite
 971 tectonique entre la plate-forme provençale et le Bassin vocontien à l'Aptien–Albien (SE France).
 972 *C. R. Geoscience*, **336**, 1301–1310.
- 973 **Morrow, D.W.** (1982) Descriptive field classification of sedimentary and diagenetic breccia
 974 fabrics in carbonate rocks. *Bull. Can. Petrol. Geol.*, **30**, 227–229.

- 975 **Murray, R.C. and Lucia, F.J.** (1967) Cause and control of dolomite distribution by rock
976 selectivity. *GSA Bull.*, **78**, 21–35.
- 977 **Nader, F.H., López-Horgue, M.A., Shah, M.M., Dewit, J., Garcia, D., Swennen, R., Iriarte, E.,**
978 **Muchez, P. and Caline, B.** (2012) The Ranero hydrothermal dolomites (Albian, Karrantza
979 Valley, Northwest Spain): implications on conceptual dolomite models. *Oil Gas Sci. Technol.*,
980 **67**, 9–29.
- 981 **Nunn, E.V. and Price, G.D.** (2010) Late Jurassic (Kimmeridgian–Tithonian) stable isotopes
982 ($\delta^{18}\text{O}$, $\delta^{13}\text{C}$) and Mg/Ca ratios: New palaeoclimate data from Helmsdale, northeast Scotland.
983 *Palaeogeogr. Palaeocl.*, **292**, 325–335.
- 984 **Ohle, E.L.** (1985) Breccias in Mississippi valley-type deposits. *Econ. Geol.*, **80**, 1736–1752.
- 985 **Phillips, W.J.** (1972) Hydraulic fracturing and mineralization. *J. Geol. Soc. London*, **128**, 337–
986 359.
- 987 **Piana, F., Musso, A., Bertok, C., d’Atri, A., Martire, L., Perotti, E., Varrone, D. and**
988 **Martinotti, G.** (2009) New data on post-Eocene tectonic evolution of the External Ligurian
989 Briançonnais (Western Ligurian Alps). *It. J. Geosci.*, **128**, 353–366.
- 990
- 991 **Podlaha, O.G., Mutterlose, J. and Veizer, J.** (1998) Preservation of $\delta^{18}\text{O}$ and $\delta^{13}\text{C}$ in belemnite
992 rostra from the Jurassic/Early Cretaceous successions. *Am. J. Sci.*, **298**, 324–347.
- 993 **Pouchou, J.L. and Pichoir, F.** (1988) Determination of mass absorption coefficients for soft X-
994 rays by use of the electron microprobe. In: *Microbeam Analysis* (Ed. Newbury D.E.), pp. 319–
995 324. San Francisco Press, San Francisco.
- 996 **Ramsay, J.G.** (1980) The crack-seal mechanism of rock deformation. *Nature*, **284**, 135–139.
- 997 **Richter, D.K., Neuser, R.D., Schreuer, J., Gies, H. and Immenhauser, A.,** (2011) Radial-
998 fibrous calcites: a new look at an old problem. *Sed. Geol.*, **239**, 23–36.
- 999 **Ronchi, P., Jadoul, F., Ceriani, A., Di Giulio, A., Scotti, P., Ortenzi, A. and Previde**
1000 **Massara, E.** (2011) Multistage dolomitization and distribution of dolomitized bodies in Early
1001 Jurassic carbonate platforms (Southern Alps, Italy). *Sedimentology*, **58**, 532–565.
- 1002 **Ronchi, P., Masetti, D., Tassan, S. and Camocino, D.** (2012) Hydrothermal dolomitization in
1003 platform and basin carbonate successions during thrusting: A hydrocarbon reservoir analogue
1004 (Mesozoic of Venetian Southern Alps, Italy). *Mar. Petrol. Geol.*, **29**, 68–89.
- 1005 **Rosenbaum, J. and Sheppard, S.M.** (1986) An isotopic study of siderites, dolomites and
1006 ankerites at high temperatures, *Geochim. Cosmochim. Acta* **50**, 1147–1150.
- 1007 **Rouire, J., Autran, A., Prost, A., Rossi, P. and Rousset, C.** (1980) Carte Géologique de la
1008 France à 1:250.000, feuille Nice (40). Bureau de Recherches Géologiques et Minières, Orléans.

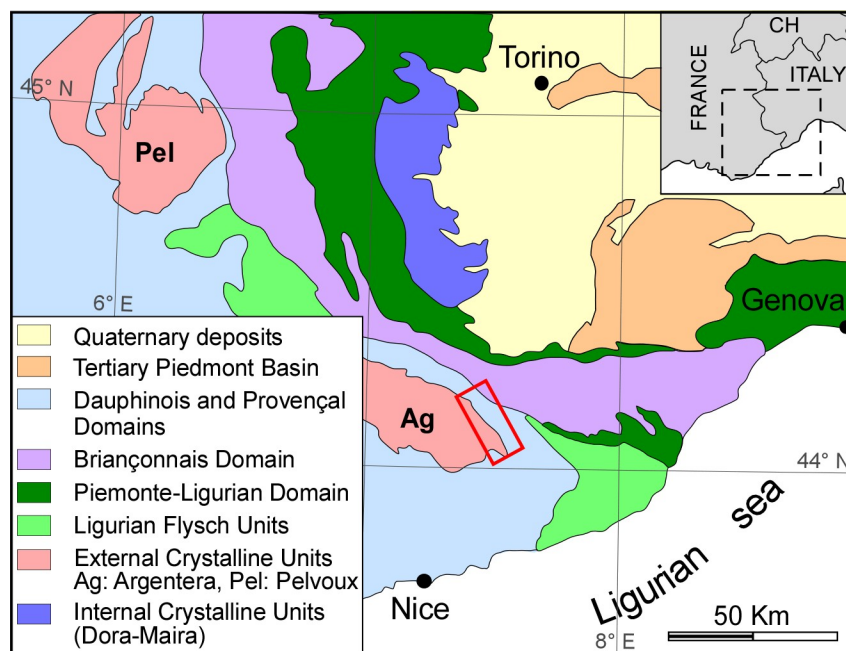
- 1009 **Schouten, S., Hopmans, E.C., Forster, A., Van Breugel, Y., Kuypers, M.M. and Sinninghe**
 1010 **Damsté, J.S.** (2003) Extremely high sea-surface temperatures at low latitudes during the middle
 1011 Cretaceous as revealed by archaeal membrane lipids. *Geology*, **31**, 1069–1072.
- 1012 **Shah, M.M., Nader, F.H., Garcia, D., Swennen, R. and Ellam, R.** (2012) Hydrothermal
 1013 dolomites in the Early Albian (Cretaceous) platform carbonates (NW Spain): nature and origin of
 1014 dolomites and dolomitizing fluids. *Oil Gas Sci. Technol.*, **67**, 97–122.
- 1015 **Sharp, I., Gillespie, P., Morsalnezhad, D., Taberner, C., Karpuz, R., Vergés, J., Horbury, A.,**
 1016 **Pickard, N., Garland, J. and Hunt, D.** (2010) Stratigraphic architecture and fracture-controlled
 1017 dolomitization of the Cretaceous Khami and Bangestan groups: an outcrop case study, Zagros
 1018 Mountains, Iran. In: *Mesozoic and Cenozoic carbonate systems of the Mediterranean and the*
 1019 *Middle East: stratigraphic and diagenetic reference models*. (Eds. F. S. P. Van Buchem, K.
 1020 Gerdes and M. Esteban), *Geol. Soc. London, Sp. Pub.*, 329, 343–396.
- 1021 **Shepherd, T. J., Rankin, A. H. and Alderton, D.H.M.** (1985) A practical guide to fluid inclusion
 1022 studies. Blackie Publishing Co., London, 239 pp.
- 1023 **Sibley, D.F.** (1982) The origin of common dolomite fabrics: clues from the Pliocene. *J. Sed.*
 1024 *Petrol.*, **52**, 1087–1100.
- 1025 **Sibley, D.F. and Gregg, J.M.** (1987) Classification of dolomite rock textures. *J. Sed. Petrol.*, **57**,
 1026 967–975.
- 1027 **Sibson, R.H.** (1987) Earthquake rupturing as a mineralizing agent in hydrothermal systems.
 1028 *Geology*, **15**, 701–704.
- 1029 **Sibson, R.H.** (1992) Implications of fault–valve behaviour for rupture nucleation and recurrence.
 1030 *Tectonophysics*, **211**, 283–293.
- 1031 **Sinclair, H.D.** (1997) Tectonostratigraphic model for underfilled peripheral foreland basins: an
 1032 Alpine perspective. *GSA Bull.*, **109**, 324–346.
- 1033 **Spencer-Cervato, C. and Mullis, J.** (1992) Chemical study of tectonically controlled
 1034 hydrothermal dolomitization: an example from the Lessini Mountains, Italy. *Geol. Rundsch.*, **81**,
 1035 347–370.
- 1036 **Stämpfli, G.M. and Marthaler, M.** (1990) Divergent and convergent margins in the north-
 1037 western Alps – Confrontation and actualistic models. *Geodin. Acta*, **4**, 159–184.
- 1038
- 1039 **Swennen, R., Dewit, J., Fierens, E., Muchez, P., Shah, M., Nader, F. and Hunt, D.** (2012)
 1040 Multiple dolomitization events along the Pozalagua Fault (Pozalagua Quarry, Basque–
 1041 Cantabrian Basin, Northern Spain). *Sedimentology*, **59**, 1345–1374.

1042 **Tugend, J., Manatschal, G. and Kuszniir, N.J.** (2015) Spatial and temporal evolution of
1043 hyperextended rift systems: Implication for the nature, kinematics, and timing of the Iberian-
1044 European plate boundary. *Geology*, **43**, 1, 15–18.

1045 **Vacherat, A., Mouthereau, F., Pik, R., Bernet, M., Gautheron, C., Masini, E., Le Pourhiet,**
1046 **L., Tibari, B. and Lahfid, A.** (2014) Thermal imprint of rift-related processes in orogens as
1047 recorded in the Pyrenees. *Earth Planet. Sci. Lett.*, **408**, 296–306.

1048FIGURE CAPTIONS

1049



1050**Fig. 1.** Schematic Geographical and geological map of the SW Alps. The red rectangle indicates
 1051the location of the study area and corresponds to Fig. 2.

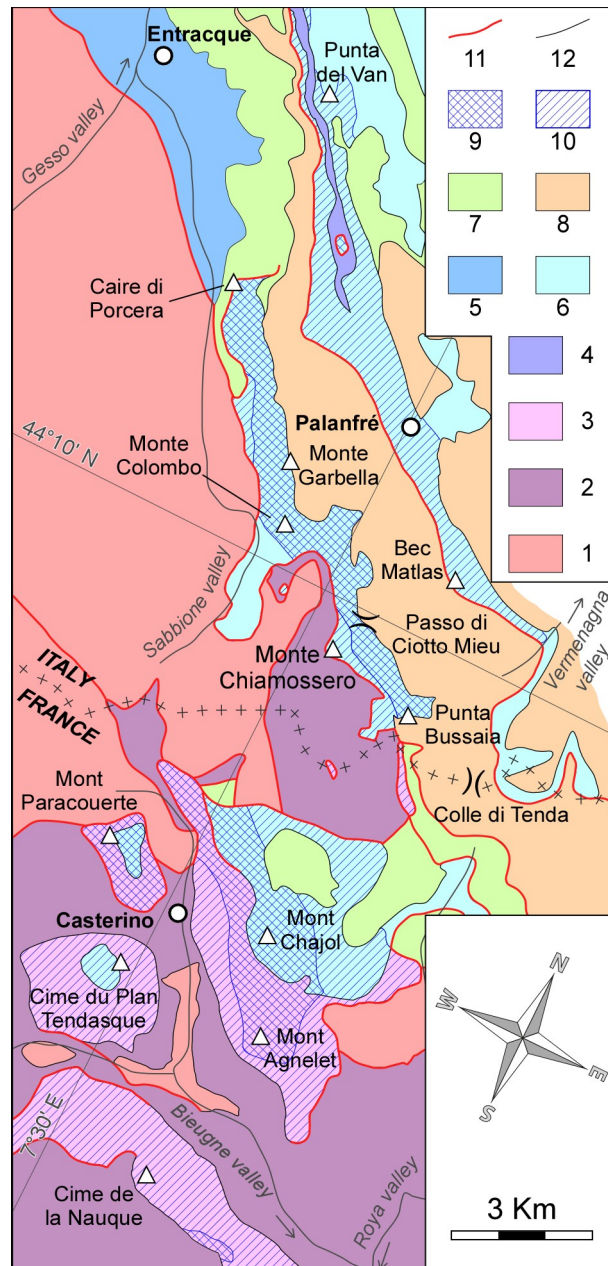
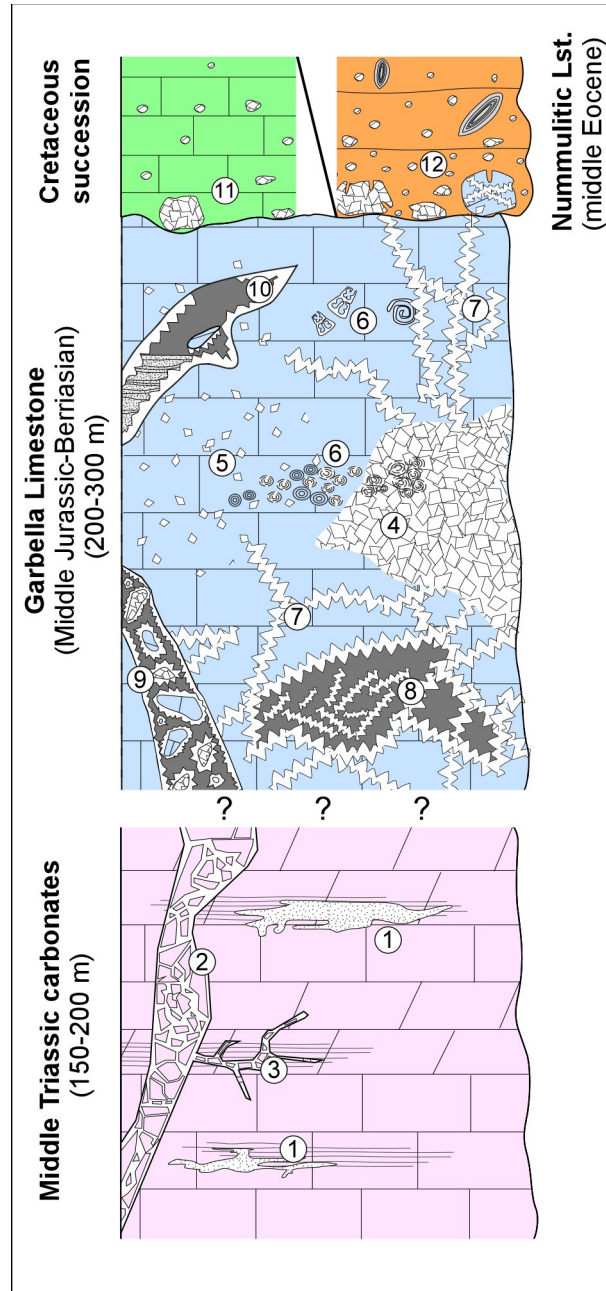


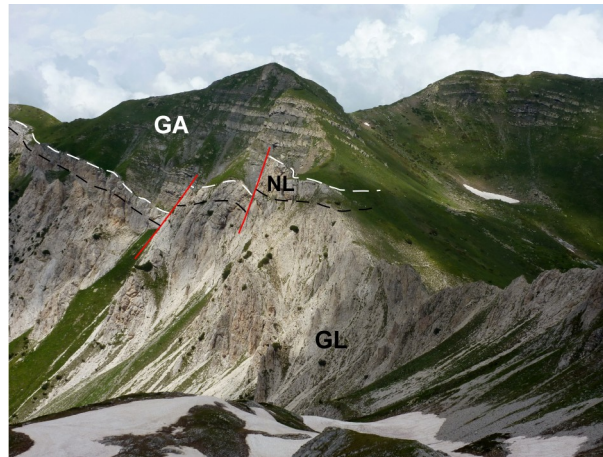
Fig. 2. Geological scheme of the study area, showing the dolomitization degree of Middle Triassic–Jurassic carbonates (the location of the study area is also reported in the geological scheme of Fig. 5). 1: Argentera Massif crystalline basement. 2: Permian–Lower Triassic siliciclastic deposits. 3: Middle Triassic carbonates. 4: Upper Triassic–Lower Jurassic succession. 5: Jurassic Dauphinois hemipelagic succession. 6: Middle Jurassic–Berriasian Provençal carbonates (Garbella Limestone). 7: Cretaceous succession. 8: Alpine Foreland Basin succession. 9: intense hydrothermal dolomitization (local complete dolomitization of the host rock; common dolomite vein frameworks and dolomite-cemented breccias). 10: moderate

1061 hydrothermal dolomitization (partial dolomitization of the host rock; rare dolomite vein networks
 1062 and dolomite-cemented breccias). 11: main faults. 12: stratigraphic contacts. Modified from:
 1063 Barale *et al.*, (2016) (Italian part); Faure-Muret *et al.*, (1967), and Lanteaume, (1990) (French
 1064 part).



1066 **Fig. 3.** Schematic stratigraphic log of the Middle Triassic–Paleogene succession in the study
 1067 area, showing the vertical distribution of the main dolomitization facies, breccia types, cavities,
 1068 and the occurrence of reworked dolomite. 1: decimetre-sized, stratabound, completely

1069dolomitized bodies. 2: subvertical bodies of type-1 breccias. 3: minor, bed-parallel type-1
 1070breccia bodies. 4: metre- to decametre-sized, completely dolomitized bodies. 5: non-selective
 1071partial dolomitization. 6: grain-selective partial dolomitization. 7: veined limestones. 8: boxwork
 1072fabrics and dolomite-vein breccias (type-4). 9: type-2 breccias. 10: dolomite-cemented
 1073dissolution cavities. 11: reworked dolomite in the Cretaceous succession. 12: reworked dolomite
 1074in the lowermost interval of middle Eocene Nummulitic Limestone.



1076**Fig. 4.** Panoramic view of the western side of Passo di Ciotto Mieu. Dolomitized Garbella
 1077Limestone (GL) are unconformably overlain by the Alpine Foreland Basin succession
 1078(Nummulitic Limestone and *Globigerina* Marl, NL; Grès d'Annot, GA). The whitish colour of the
 1079Garbella Limestone reflects a high degree of dolomitization. The cliff of Garbella Limestone in
 1080the centre of the image is about 100 metres high; image taken from Monte Chiamossero
 1081eastern side (44°09'29.0"N, 7°30'44.8"E), looking north.

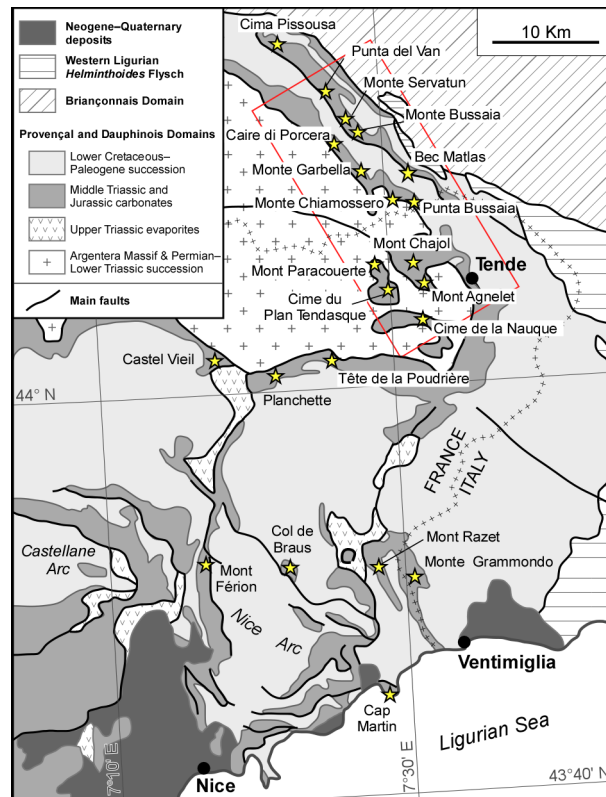


Fig. 5. Geological scheme of the French–Italian southern Maritime Alps (redrawn from Rouire *et al.*, 1980), showing the distribution of the hydrothermal dolomite outcrops (stars). The red rectangle indicates the location of the study area and corresponds to Fig. 2.

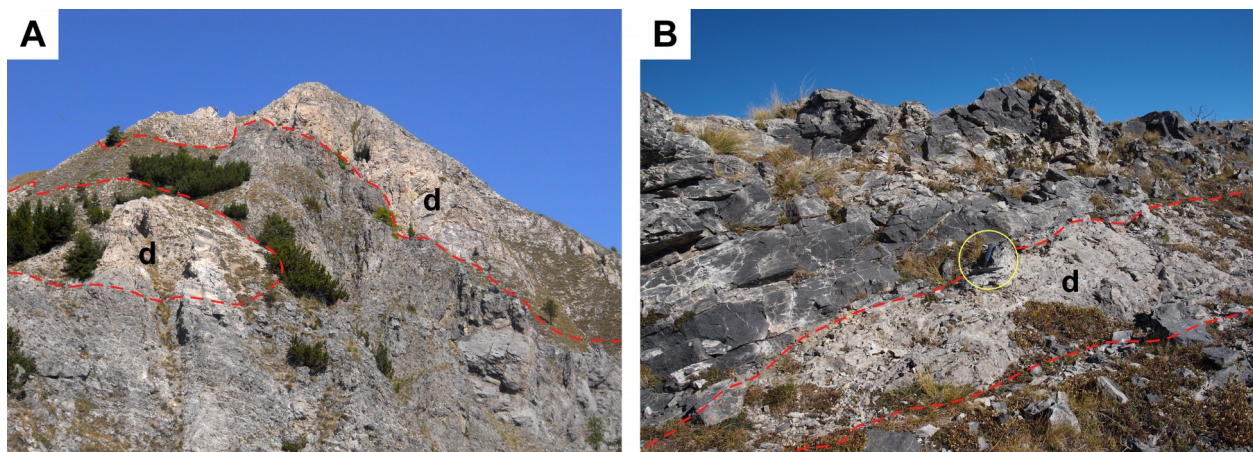


Fig. 6. Field features of dolomitized rock bodies. (A) Discontinuous, decametre-thick, white-coloured, pervasively dolomitized rock bodies (d) within the grey-coloured, partially dolomitized Upper Triassic–Jurassic carbonates on Mont Chajol southern side. The image shows a portion of cliff about 110 metres high, and has been taken from Mont Chajol southern ridge

1091(44°05'58.4"N, 7°31'50.6"E), looking north. (B) Stratabound, decimetre-thick, completely
 1092dolomitized rock body (d) in the Middle Triassic carbonates of Mont Agnelet (44°05'14.3"N,
 10937°31'56.5"E); encircled hammer for scale.

1094



1095**Fig. 7.** Complex network of decimetre-thick, tabular bodies of dolomite-cemented breccia in
 1096evenly bedded Middle Triassic carbonates (Mont Paracouerte southern side; 44°06'14.5"N,
 10977°29'05.9"E); breccia bodies either crosscut at a high angle the host-rock bedding or develop
 1098parallel to it.

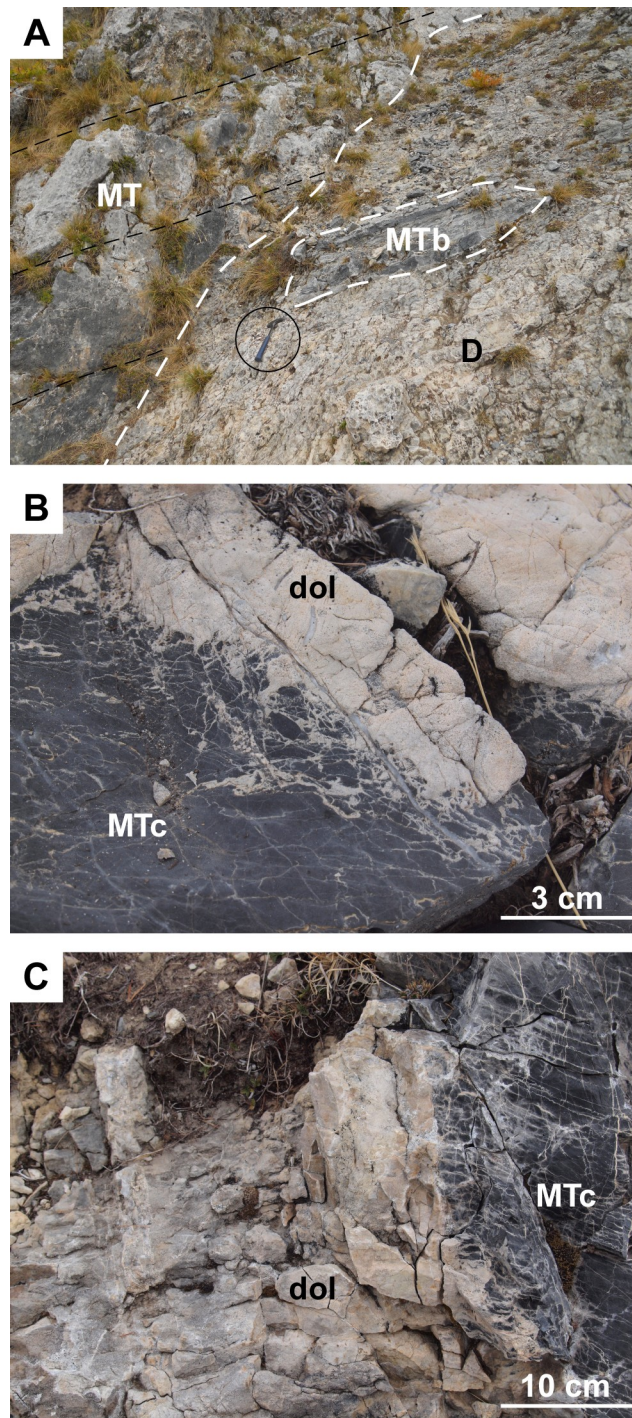
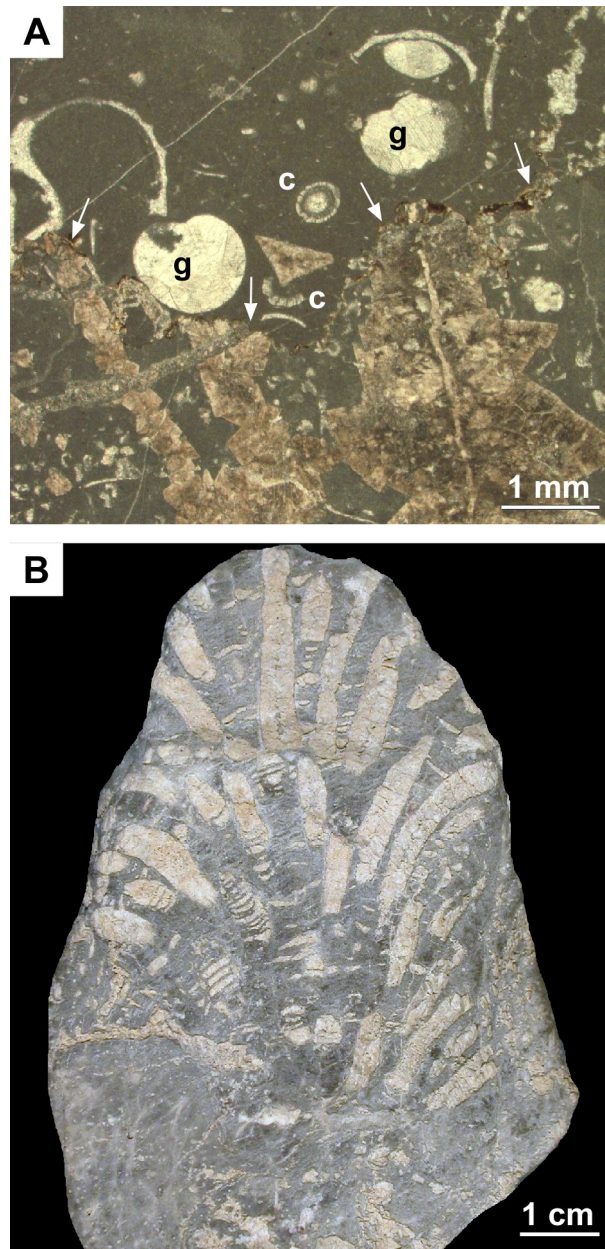


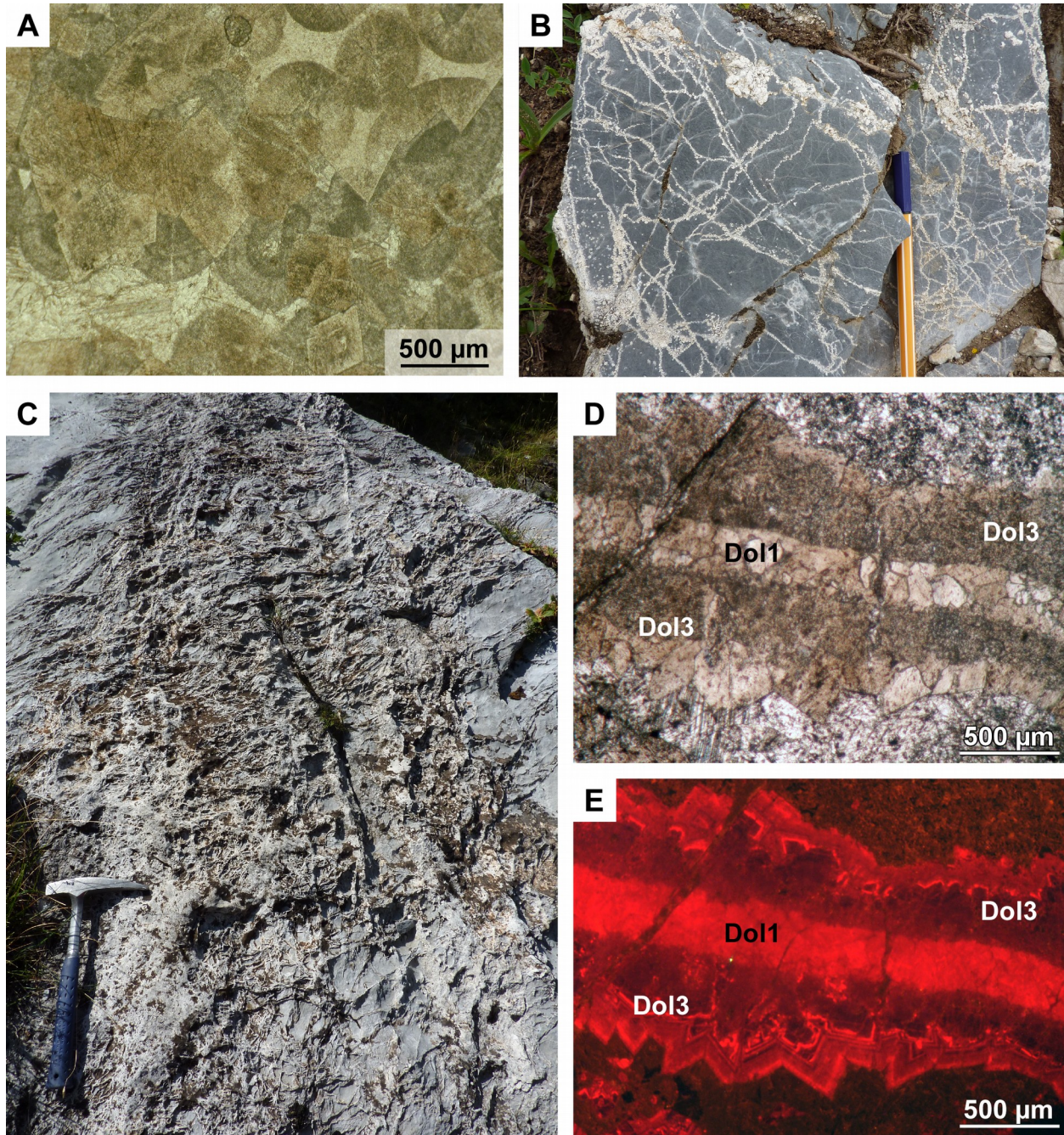
Fig. 8. (A) Subvertical body made up of coarsely to very coarsely crystalline dolostones and dolomite-cemented breccias (D), showing a sharp contact with the poorly dolomitized Middle Triassic host rock (MT) and embedding a metre-sized, angular block of the same Middle Triassic carbonates (MTb); Mont Agnelet (44°05'16.5"N, 7°31'53.0"E). Black lines indicate the bedding of Middle Triassic carbonates (encircled hammer for scale). (B) Stratabound,

1102decimetre-thick, light-coloured, completely dolomitized body (dol) within Middle Triassic
 1103carbonates (MTc), showing an incipient nodular structure. At the boundary of the dolomitized
 1104body, dolomitization affects the internodular matrix but not the nodules themselves (Mont
 1105Agnelet; 44°05'13.6"N, 7°31'57.0"E). (C) Subvertical, light-coloured, completely dolomitized
 1106body (dol) within Middle Triassic carbonates (MTc), showing a sharp contact with the host rock.
 1107Mont Agnelet (44°05'14.3"N, 7°31'56.8"E).



1109**Fig. 9.** (A) Transmitted-light photomicrograph showing a bedding-parallel, burial stylolite
 1110(arrows) which separates a bioclastic wackestone crossed by dolomite veins (in the lower part)

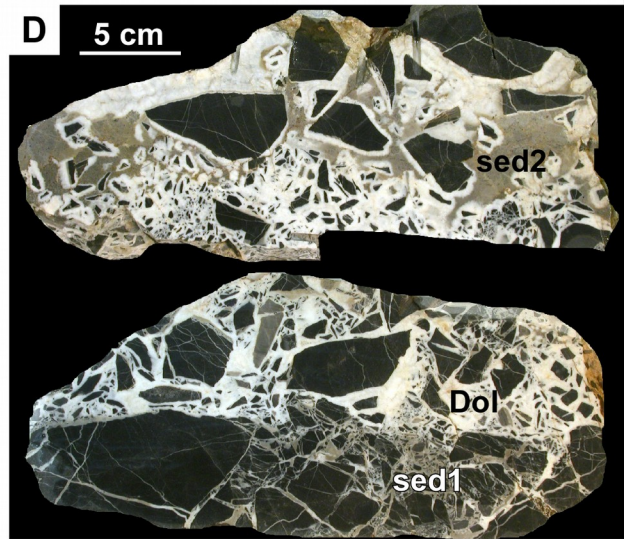
1111 from an undolomitized bioclastic wackestone with gastropod moulds (g), charophytae
 1112 gyrogonites (c), and other bioclasts (in the upper part). Note that dolomite veins are clearly cut
 1113 by the stylolite. Upper part of the Garbella Limestone, Monte Colombo. (B) Selective
 1114 replacement of corals in a coral boundstone (Garbella Limestone, Sabbione Valley).
 1115



1117

Fig. 10. Partial-dolomitization fabrics: (A) Transmitted-light photomicrograph showing a non-selective dolomitization of an ooidal grainstone: euhedral dolomite crystals grow indifferently on the ooids and on the cement. (B) Network of dolomite veins crossing the Garbella Limestone (Passo di Ciotto Mieu; 44°09'47.9"N, 7°30'46.1"E). A few isolated dolomite crystals also occur in the host rock. (C) Sub-vertical, decimetre-wide, tabular rock volume characterized by a very high density of dolomite veins, crossing the Garbella Limestone (Palanfré; 44°10'28.1"N, 47°29'44.0"E). (D), (E) Transmitted-light photomicrograph (D) and cathodoluminescence image (E) of a dolomite vein crossing the Garbella Limestone, showing a thin inner part composed of medium crystalline, turbid dolomite (Dol1), and a thicker outer part composed of outward growing, coarse dolomite crystals (Dol3).

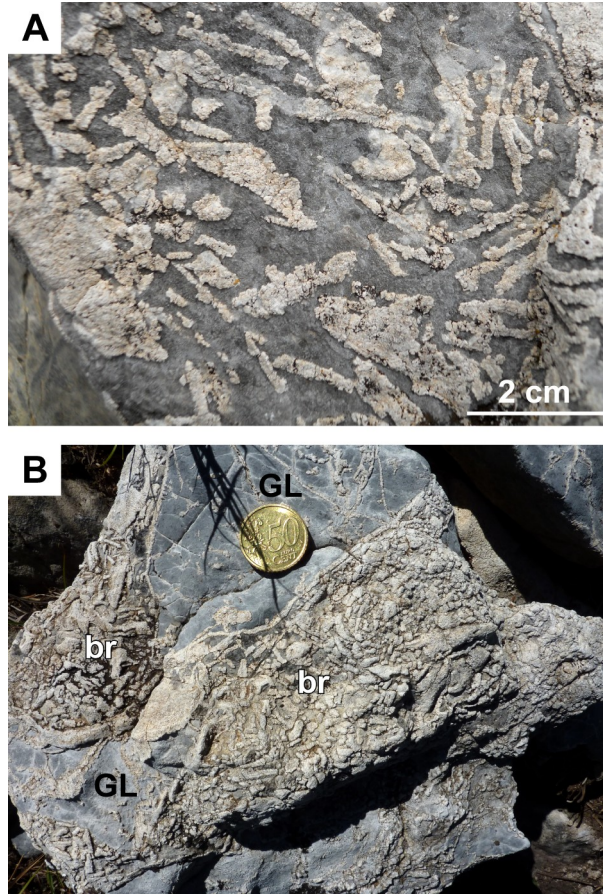
1129



1130

1131**Fig. 11.** Breccia features: (A) Centimetre-large, tabular breccia body crossing the bedding of
 1132finely laminated Middle Triassic carbonates at a high angle (fallen block on Mont Paracouerte
 1133western side; 44°06'10.8"N, 7°29'03.3"E). (B) Irregularly shaped, metre-sized breccia body in
 1134Middle Triassic carbonates (Mont Paracouerte; 44°06'14.4"N, 7°29'06.9"E). (C) Type-1 breccia
 1135in Middle Triassic carbonates, made up of centimetre-sized, angular clasts showing a jigsaw-
 1136puzzle arrangement (Mont Agnelet; 44°05'12.0"N, 7°31'58.5"E). (D) Two polished hand samples
 1137(juxtaposed in their relative position) of a type-1 breccia, made up of clasts of Middle Triassic
 1138carbonates, and showing a complex void filling. In the lower part, voids between clasts are filled
 1139with a grey, micritic sediment (sed1), which is followed by a white dolomite cement (Dol), in turn
 1140followed by a micritic, brownish sediment in the upper part (sed2) (Cime du Plan Tendasque;
 114144°05'27.4"N, 7°29'49.0"E). (E) Tabular body of type-1 breccia crossing a veined volume of
 1142Garbella Limestone (Sabbione Valley; 44°10'13.6"N, 7°28'37.5"E). Note the gradual transition
 1143between the breccia body and the veined limestones, occurring by a progressive increase of
 1144clast displacement resulting in the formation of centimetre-wide voids filled with coarse dolomite
 1145cement. (F) Type-1 breccia composed of centimetre-sized clasts of Middle Triassic carbonates,
 1146in turn locally crossed by millimetre-thick dolomite veins (fallen block on Mont Paracouerte
 1147western side; 44°06'13.7"N, 7°28'53.6"E). (G) Type-2 breccia, consisting of centimetre-sized,
 1148subrounded clasts of coarsely crystalline dolostones. Voids between clasts are cemented by a
 1149millimetre- to centimetre-thick rim of coarsely to very coarsely crystalline, white dolomite, with
 1150dark-coloured calcite plugging the remaining pores (near Passo di Ciotto Mieu; 44°09'51.1"N
 11517°31'12.1"E). (H) Type-3, polymictic, clast-supported breccia with centimetre-sized, angular to
 1152subrounded, clasts, composed of dolostones, limestones and partially dolomitized limestones, in
 1153a micritic matrix containing sand-sized clasts of the same lithologies as larger clasts (Passo di
 1154Ciotto Mieu; 44°09'49.6"N, 7°30'48.2"E).

1155



1156**Fig. 12. Breccia features:** (A) Close-up view of a type-4 breccia, mostly composed of
 1157millimetre- to centimetre-long and millimetre-wide, plate-like clasts made up of coarsely
 1158crystalline dolomite. Voids between clasts are cemented by dark-grey, sparry calcite (eastern
 1159side of Sabbione valley). (B) Centimetre-large tabular bodies of type-4 breccia (br), bordered by
 1160veins in the host Garbella Limestone (GL) (Monte Colombo).

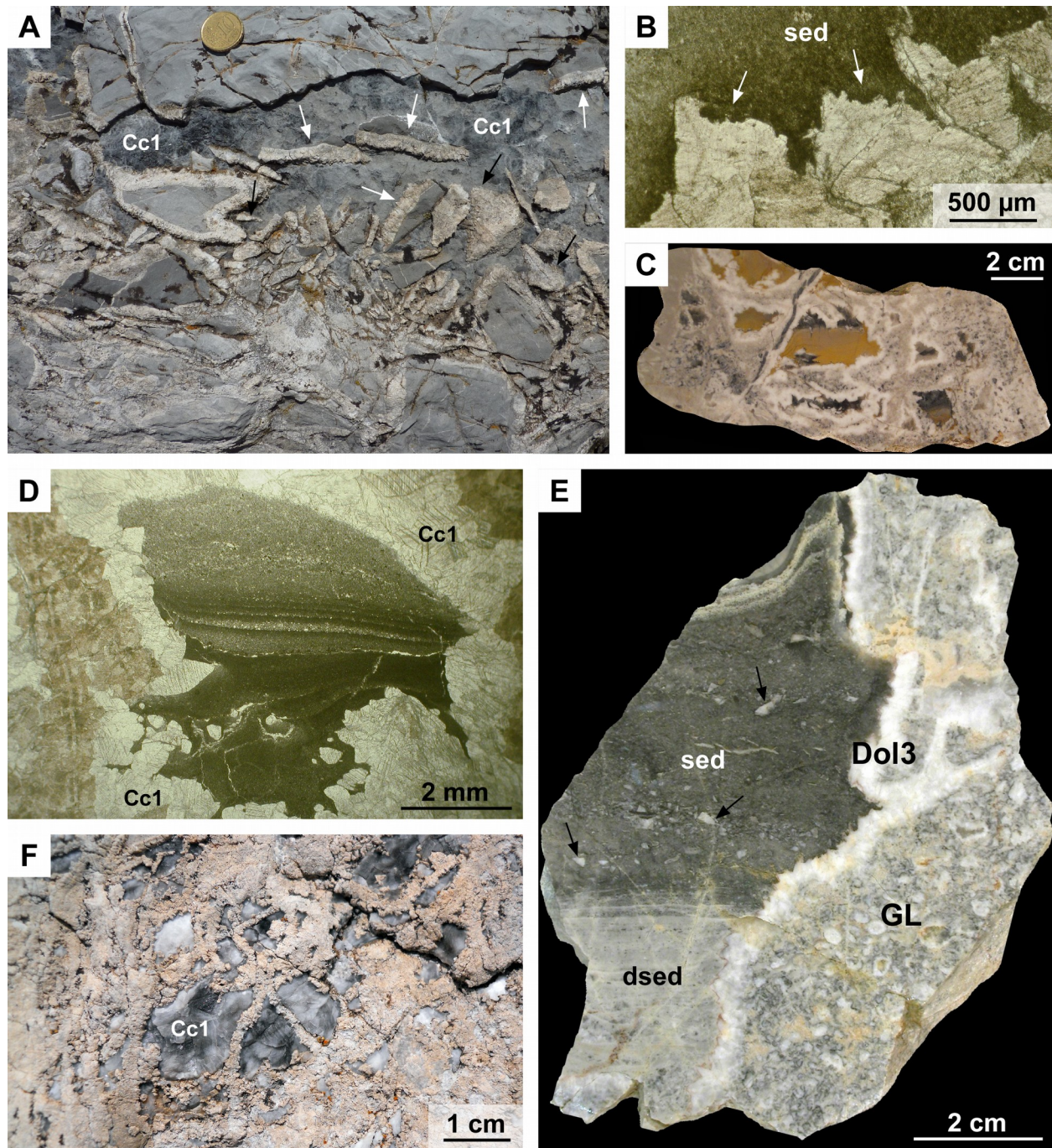
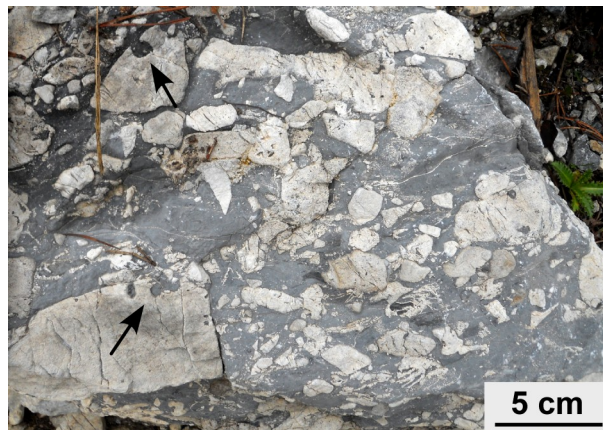


Fig. 13. Cavity features: (A) Large dissolution cavity in Middle Triassic carbonates. The occurrence of clasts with asymmetric white, very coarsely crystalline dolomite cement rims (saddle dolomite Dol 3, white arrows) and clasts entirely made up of the same dolomite cement (black arrows) indicate that cavity walls were fractured after precipitation of a coarse dolomite cement rim on them and before being plugged by a dark-coloured sparry calcite (Cc1). (Monte Chiamossero; 44°09'28.6"N, 7°30'50.5"E). (B) Transmitted-light photomicrograph showing a

1164 portion of a dissolution cavity rimmed by a coarsely crystalline dolomite cement (saddle
 1165 dolomite Dol3), and filled by a fine-grained sediment (sed). Note the jagged outline of dolomite
 1166 crystals (arrows), due to dissolution of crystal faces. (C) Polished hand sample showing
 1167 centimetre-sized cavities within completely dolomitized Garbella Limestone, rimmed by a white,
 1168 very coarsely crystalline dolomite cement (saddle dolomite Dol3) and filled by mustard-coloured
 1169 internal sediments, giving rise in some cases to geopetal structures plugged by a sparry dark-
 1170 coloured calcite cement (Cc1) (eastern side of Sabbione Valley). (D) Transmitted-light
 1171 photomicrograph of a centimetre-sized cavity hosting silt-sized internal sediments, locally
 1172 organized into graded laminae. Cavity walls are rimmed by a sparry calcite cement (Cc1). (E)
 1173 Polished hand sample showing a large dissolution cavity in partially dolomitized bioclastic-
 1174 oncoidal rudstones of the Garbella Limestone (GL). The cavity is rimmed by a white, very
 1175 coarsely crystalline dolomite cement (saddle dolomite Dol3) and filled by two different
 1176 sediments. A first layer of laminated, dolomitized sediment (dsed) is followed by a second one
 1177 of undolomitized sediment (sed), containing fragments of Dol3 crystals (arrows) (Monte
 1178 Chiamossero; 44°09'36.0"N, 7°31'24.8"E). (F) Boxwork fabric in the Garbella Limestone:
 1179 centimetre-sized cavities, filled with a sparry, locally dark-coloured, calcite cement (Cc1), are
 1180 divided by a complex 3D network of thin dolomite veins. (Passo di Ciotto Mieu; 44°09'48.6"N,
 1181 17°30'45.4"E).

1182



1183 **Fig. 14.** Upper surface of a conglomerate bed in the basal interval of the Nummulitic Limestone,
 1184 made up of clasts of dolomitized Garbella Limestone locally showing *Gastrochaenolites* bivalve
 1185 borings (arrows). (Monte Garbella; 44°10'12.9"N, 7°28'39.8"E).

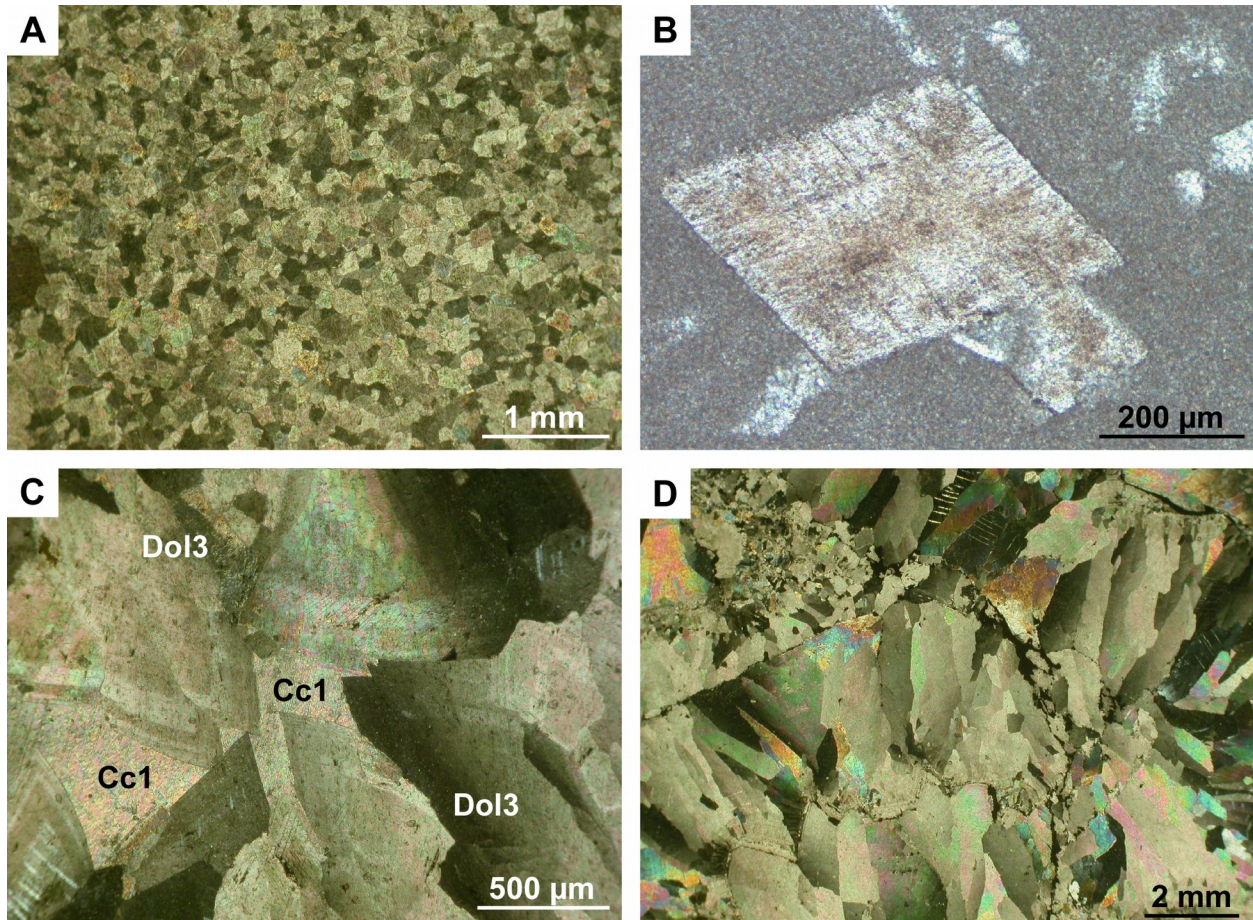


Fig. 15. (A) Transmitted-light, crossed polars photomicrograph of a Garbella Limestone sample, fully dolomitized by finely to medium crystalline, subhedral Dol1 replacement dolomite. (B) Transmitted-light photomicrograph showing a coarse, euhedral crystal of Dol2 replacement dolomite, growing in a mudstone bed of the Garbella Limestone. (C) Transmitted-light, crossed polars photomicrograph showing a detail of a cavity cemented by coarsely to very coarsely crystalline, Dol3 saddle dolomite, with Cc1 calcite plugging the remaining voids. Note: the curved crystal faces, the zoning, and the sweeping extinction of Dol3. (D) Transmitted-light, crossed polars photomicrograph showing very coarsely crystalline fascicular-optic Dol4 dolomite cements. Note the sweeping extinction of the crystals.

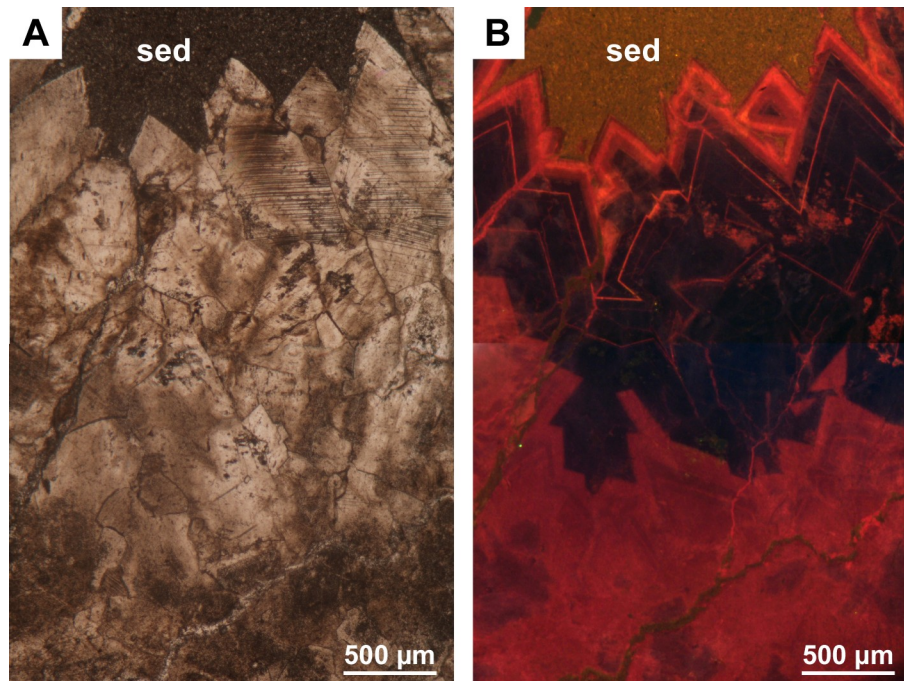


Fig. 16. Transmitted light (A) and cathodoluminescence (B) photomicrographs of a very coarsely crystalline, Dol3 saddle dolomite rimming a cavity, and overlain by a fine-grained, calcitic sediment (sed). Dol3 crystals have a thick inner part with dull to moderate red–orange luminescence, followed by a thick non-luminescent zone with hairline, moderately to brightly luminescent, orange zones, and by an outer part with moderate to bright, red–orange luminescence zones.

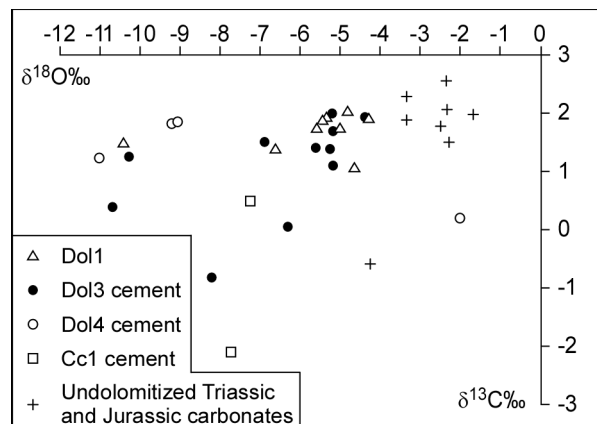


Fig. 17. Stable isotope data: $\delta^{18}\text{O}$ versus $\delta^{13}\text{C}$ cross-plot for Dol1, Dol3 and Dol4 dolomite, for Cc1 calcite, and for Triassic and Jurassic host carbonates (values relative to VPDB standard).

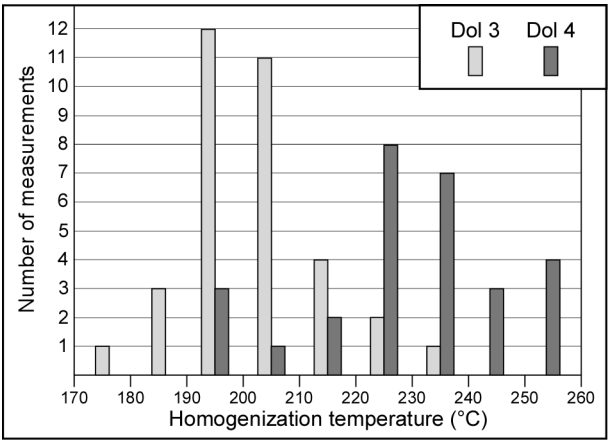


Fig. 18. Histogram of the homogenization temperatures obtained for Dol3 saddle dolomite and for Dol4 cements.

1209

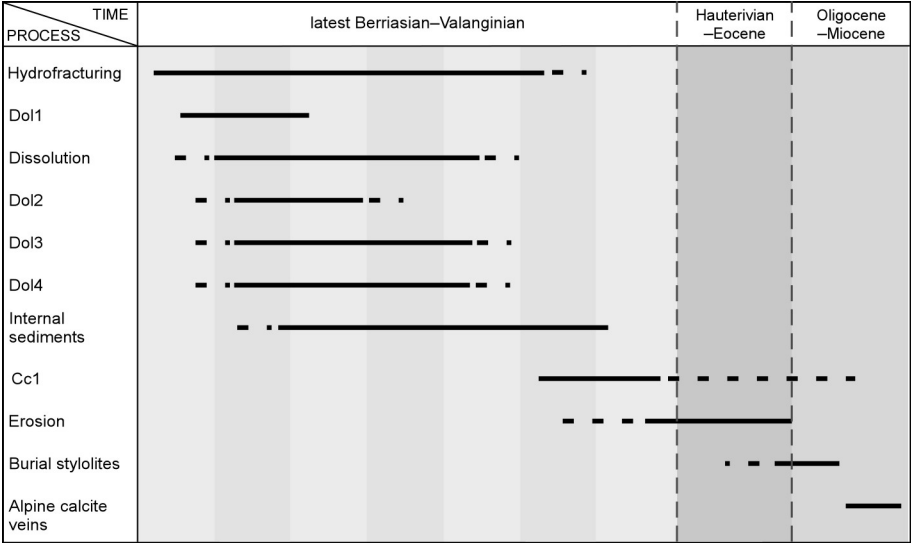


Fig. 19. Schematic paragenetic sequence showing the relative timing of the processes that affected the host rocks during and after hydrothermal dolomitization. Dashed lines indicate the uncertainty range.

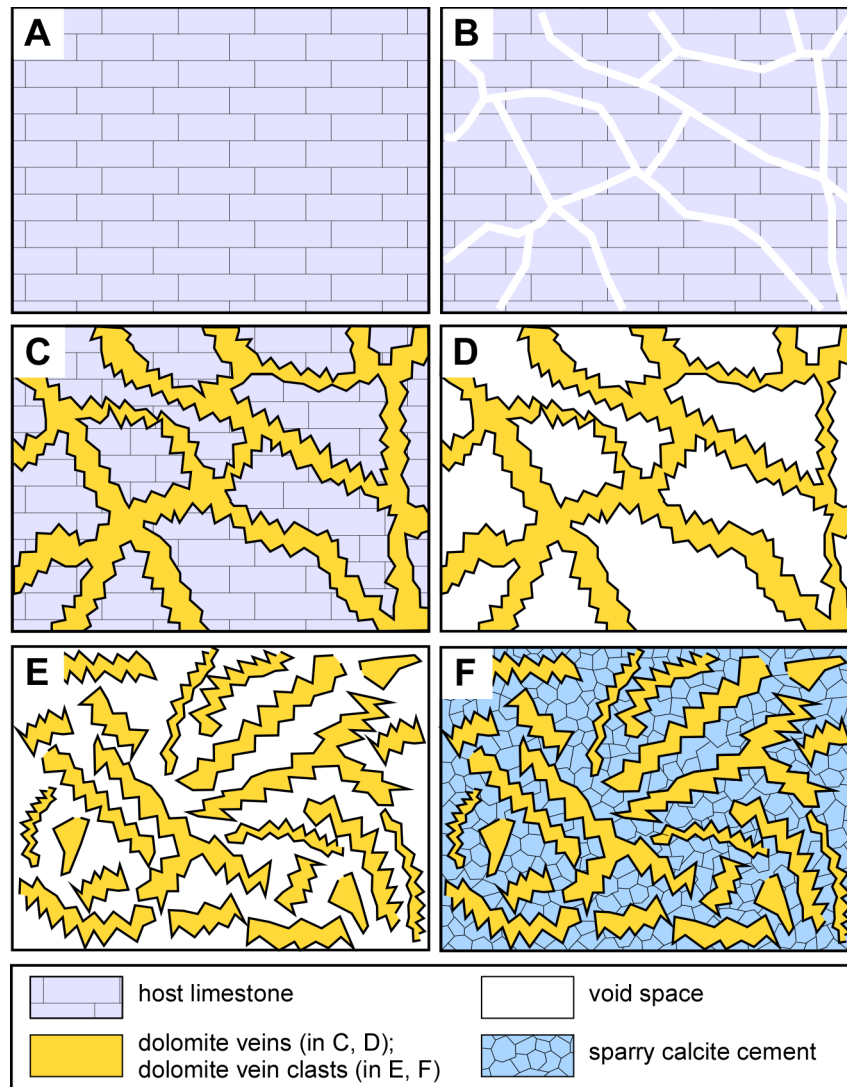


Fig. 20. (A–F) Interpretive sketch of the different steps leading to the formation of the type-4 breccias. A, B: the host limestone is crossed by a network of thin fractures. C: dolomitizing fluids flow through the fractures, resulting in dolomite cementation of the fractures and dolomitization of their walls. D: a local but complete dissolution of the host limestone occurs, leaving a frail network of isolated dolomite veins. E: the vein network collapses, forming clasts of vein material. F: clasts are cemented by sparry calcite.

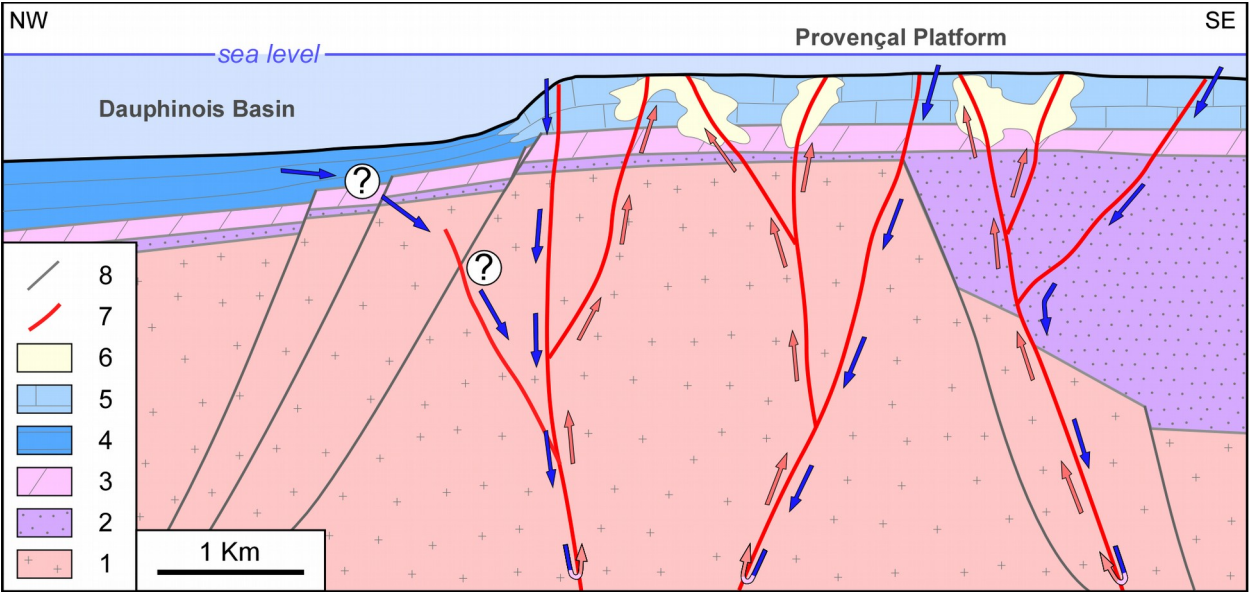
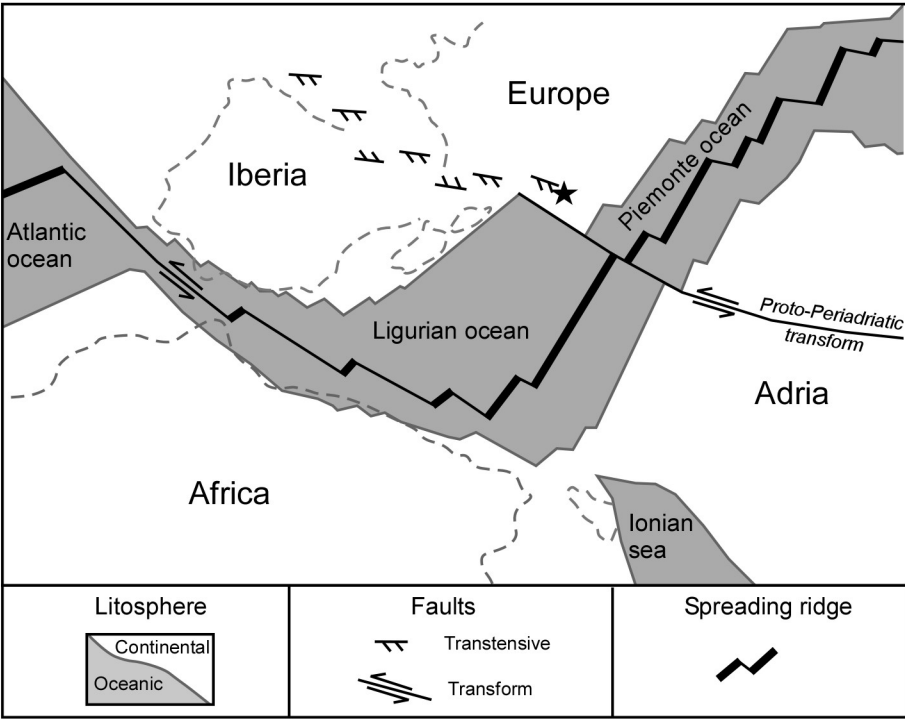


Fig. 21. Conceptual model illustrating the geometries of the hydrothermal system, and the hypothetical origin and circulation pathways of the fluids. Blue arrows represent cold descending fluids, whereas red arrows represent hot ascending fluids. Legend: 1: Argentera Massif crystalline basement. 2: Permian–Lower Triassic siliciclastic deposits. 3: Middle Triassic carbonates. 4: Jurassic Dauphinois hemipelagic succession. 5: Middle Jurassic–Berriasian Provençal carbonates (Garbella Limestone). 6: dolomitized bodies. 7: Early Cretaceous, syn-dolomitization faults. 8: inherited, Early Jurassic and Palaeozoic faults.



1229**Fig. 22.** Palaeogeographic sketch of the Western Mediterranean area in the Early Cretaceous.
1230The black star indicates the position of the study area. Modified after Handy *et al.* (2010).